LOS ALAMOS SCIENTIFIC LABORATORY

OF THE

UNIVERSITY OF CALIFORNIA

CONTRACT W-7405-ENG. 36 WITH

U. S. ATOMIC ENERGY COMMISSION

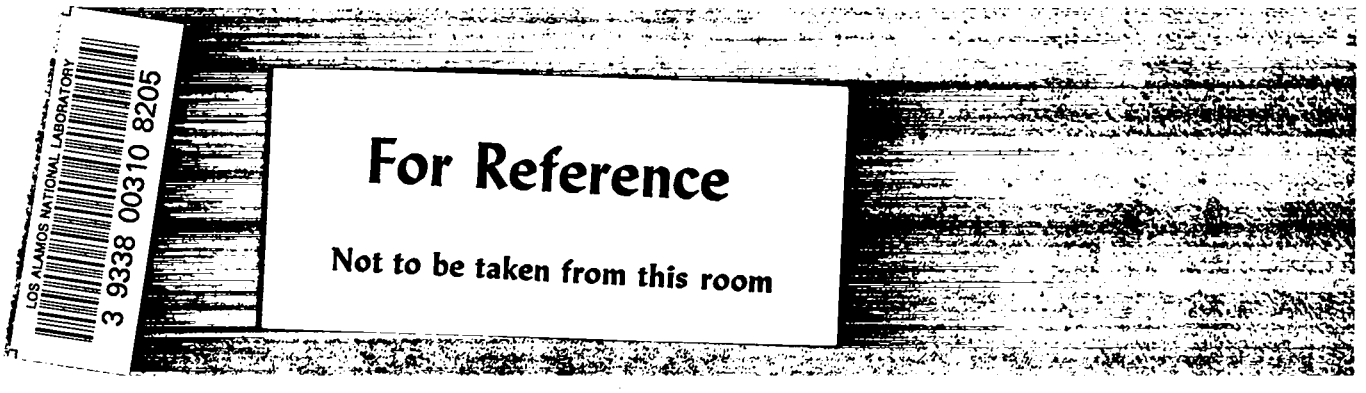

c. 3

LOS ALAMOS SCIENTIFIC LABORATORY
of the
UNIVERSITY OF CALIFORNIA

Report written:
November 1953

LA-1600

Report distributed: FEB 1 1954

EXPERIMENTAL STUDIES OF TAYLOR INSTABILITY

Work done by:
John C. Allred
George H. Blount
John H. Miller, III

Report written by:
John C. Allred
George H. Blount

PHYSICS

ABSTRACT

Experimental observations of Taylor instability have been made on interfaces of fluids under uniform and under impulsive accelerations. The theoretical results of Pennington and Bellman and of Birkhoff and Ingraham concerning the effects of surface tension and viscosity on the growth of Taylor instability were investigated. Inhibition of growth by surface tension is found to be in essential agreement with the theory. The growth coefficients, α ($\eta = \eta_0 \cosh \alpha t$), were measured to be less than those predicted by the linear theory in cases where growth of a wave was observed. The discrepancy is perhaps due to effects connected with the necessarily finite amplitude of the wave when measurements can be made.

A new mechanism leading to the restraint of growth is proposed, that of the existence of a density gradient of finite width at an interface, as opposed to a true discontinuity of density. The importance of Helmholtz instability in the development of the shape of the interface is demonstrated. Turbulent mixing of the fluids at sufficiently great Reynolds number is observed. The mixing, producing a region of density gradient, provides a final inhibitory effect on the growth.

The wavelength of most rapid growth at an interface has been observed in experiments with impulsive acceleration, again in agreement with theory. Some experimental refinements for future observations of impulsive accelerations are suggested.

ACKNOWLEDGMENT

The work described in this report was undertaken at the behest, primarily, of Conrad Longmire and J. L. Tuck, to whom we are indebted for their continued interest and helpful discussions.

On account of the many specialized techniques which were required, we had need for consultation with various members of the Laboratory. A complete list would be long indeed, but we feel obliged to list the following as having been of great assistance in various phases of the work: Garrett Birkhoff, W. L. Briscoe, Berlyn Brixner, W. E. Buck, P. W. Byington, D. S. Carter, and R. E. Duff.

We wish also to note our appreciation of the very helpful cooperation of the Graphic Arts Group, under Loris Gardner and J. D. Elliott, and to Catherine Lacey and Opal Milligan of the Nuclear Microscopy Group for their assistance in analyzing the data.

CONTENTS

ILLUSTRATIONS

ILLUSTRATIONS (Cont.)

ILLUSTRATIONS (Cont.)

Chapter 1

THE THEORY OF TAYLOR INSTABILITY

1.1 Potential Theory as Applied to Hydrodynamics

The equation of motion of a perfect fluid is[1]

$$\rho \frac{\partial v}{\partial t} + \rho v \cdot \nabla v = \rho F - \nabla p + 1/3\ \mu \nabla \nabla \cdot v + \mu \nabla \cdot \nabla v \tag{1.1}$$

where ρ is the density, v the velocity, F the body force (per unit mass), and μ the coefficient of viscosity. The equation of continuity is

$$\frac{d\rho}{dt} + \rho \nabla \cdot v = 0 \tag{1.2}$$

It can also be shown that the vorticity, ω, is given by

$$\omega = \frac{1}{2} \nabla x v \tag{1.3}$$

A very powerful method in hydrodynamics is that of potential theory, which enters when the motion is assumed to be irrotational and incompressible. For then

$$\frac{d\rho}{dt} = 0 \text{ and} \tag{1.4}$$

$$\nabla \cdot v = 0 \tag{1.5}$$

Further, since $\nabla x v = 0$, v is derivable from a scalar potential ϕ, owing to the vector identity $\nabla x \nabla \phi = 0$.

Hence

$$v = -\nabla \phi \tag{1.6}$$

where the negative sign is conventional and ϕ is called the velocity potential. ϕ satisfies Laplace's equation

$$\nabla^2 \phi = 0 \tag{1.7}$$

Under the conditions of incompressible, irrotational flow the equation of motion (1.1) becomes

$$\rho \frac{\partial v}{\partial t} + \rho v \cdot \nabla v = \rho F - \nabla p + \mu \nabla \cdot \nabla v \tag{1.8}$$

If we neglect viscosity and assume F to be derivable from a potential Ω (usually the gravitational potential), we can integrate the equation of motion to obtain Bernoulli's equation

$$\frac{p}{\rho} = \frac{\partial \phi}{\partial t} - \Omega - 1/2\ v^2 + f(t) \qquad (1.9)$$

We note that if the motion is steady, f(t) is a constant.

Hence the solution for the velocity potential in irrotational, incompressible flow is that solution of Laplace's equation which satisfies (1.9) together with the physical boundary conditions.

Sir Geoffrey Taylor[2] has used the potential theory to discuss the motion of the interface between two incompressible fluids in a gravitational field, neglecting surface tension and viscosity. His result is that an infinitesimal sinusoidal displacement of initial amplitude η_0 grows as

$$\eta = \eta_0 \cosh \alpha t$$

where $\alpha = \left[kg \frac{\rho_2 - \rho_1}{\rho_2 + \rho_1} \right]^{1/2}$, provided $\rho_2 > \rho_1$ and the gravitational field is directed from ρ_2 toward ρ_1.*

Taylor's solution neglects the term $\frac{\rho v^2}{2}$ in Bernoulli's equation in order to linearize the theory. This term has likewise been neglected by subsequent workers, although its effect is perhaps important in the development of asymmetries in the interface, as we shall presently suggest.

1.2 Derivation of Instability Criteria

Rigorous mathematical discussions of the Taylor instability are to be found in the literature and will not be repeated here. It is possible, however, to give approximate derivations which lead to the same results and possibly give more physical insight into the effects of various quantities than do the more elegant presentations.

To this end, let us consider the equation of motion of an interface in an acceleration field of magnitude g, as indicated in the sketch. If η is the displacement of the interface, the restoring force will be of the order of

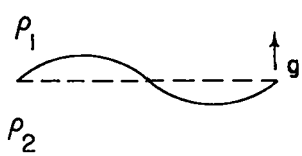

$$f = -\eta \lambda g(\rho_2 - \rho_1)$$

and the mass which must be moved is, approximately, $(\rho_2 + \rho_1)\lambda^2$, since the circulation in a wave is of depth of order λ.

*We may here observe that the effect of a gravitational field is completely equivalent to the acceleration of a system in a direction opposite to that of the gravitational force. Hence we may say that the interface is unstable if the acceleration is directed from the lighter to the denser medium or, equivalently, when the gravitational field is directed from the denser to the lighter medium.

Equating

$$ma = f$$

$$(\rho_2 + \rho_1)\lambda^2\ddot{\eta} = -\eta\lambda g(\rho_2 - \rho_1)$$

and since $\lambda = k^{-1}$

$$\ddot{\eta} = -kg\frac{\rho_2 - \rho_1}{\rho_2 + \rho_1}\eta$$

If we set $\alpha^2 = -kg\frac{\rho_2 - \rho_1}{\rho_2 + \rho_1}$ the solutions are

$$\eta = C_1 e^{\alpha t} + C_2 e^{-\alpha t}$$

Hence if the acceleration field is directed upward, α is imaginary and the solutions are oscillatory. But if the direction of g is reversed, α is real and the solutions are exponential functions.

Since we wish to describe an interface with finite initial displacement and initial velocity zero, we arrive at $C_1 = C_2 = \eta_o/2$, and $\eta = \eta_o \cosh \alpha t$, as in Taylor's theory.

We have now to consider the effects of surface tension and viscosity on the stability of the interface. We may again calculate by an approximate method the effect of surface tension and arrive at the same result as that attained independently by Pennington[3] and by Birkhoff and Ingraham,[4] all of whom used more rigorous methods.

Consider now the increase in gravitational energy resulting from the displacement of a flat interface to the form $\eta = \eta_o \sin kx$. If we take the thickness of the interface as unity, the displaced volume of a half-wave is

$$V = \int_o^{\lambda/2} \eta \cdot dx = \frac{\eta_o}{k}$$

and the mean displacement is

$$\bar{\eta} = \frac{\int_o^{\lambda/2} \eta^2\, dx}{\int_o^{\lambda/2} \eta\, dx} = \frac{\pi}{2}\eta_o$$

Hence the change in gravitational energy is

$$\Delta E_g = (\rho_2 - \rho_1) \frac{\eta_o}{k} g \frac{\eta_o \pi}{2} = \frac{\pi}{2k} (\rho_2 - \rho_1) \eta_o^2$$

The surface area of the interface is, for unit thickness, initially λ. With the distortion the area becomes

$$A = \int_o^\lambda ds = \int_o^\lambda (1 + \eta_o^2 k^2 \cos^2 kx)^{1/2} dx$$

Expanding and neglecting higher order terms (since $\eta_o k << 1$), we obtain

$$A = \lambda + \frac{\pi \eta_o^2 k}{2}$$

$$\Delta A = \frac{\pi \eta_o^2 k}{2}$$

and the change in energy at the surface due to surface tension is

$$\Delta E_T = T \Delta A$$

$$= \frac{\pi \eta_o^2 k T}{2}$$

It is clear that the surface will be stable if a displacement tends to increase its total energy; that is, if the increased energy due to surface tension is greater than the decrease of energy in the gravitational field. We may then write the condition for stability

$$\Delta E_T > \Delta E_g$$

$$\frac{\pi \eta_o^2 k T}{2} > \frac{\pi}{2k} (\rho_2 - \rho_1) \eta_o^2 g$$

$$k^2 > \frac{(\rho_2 - \rho_1) g}{T}$$

We see that there exists a wave number beyond which instability ceases. We might expect that at all wave numbers the effect of surface tension would be to decrease α. Pennington[3] has shown rigorously that this is the case.

The effect of viscosity in the linear theory is a degree more subtle. To understand the effect of viscosity we need only observe that the presence of viscosity in a liquid gives rise

to dissipation of energy as the laminae of fluid move in shear. If the wave number is infinite we will have infinite dissipation of energy as the interface begins its growth. Hence we may expect that at all wave numbers the effective α will be reduced by viscous effects and that for infinite wave number α becomes zero and no growth occurs.

Pennington[3] has shown that in the linear theory α is a root of

$$\left[g(\rho_2 - \rho_1)k + Tk^3 + (\rho_1 + \rho_2)\alpha^2 \right] x$$

$$\left[\frac{1}{\mu_1 k + \sqrt{\mu_2^2 k^2 + \mu_2 \rho_2 \alpha}} + \frac{1}{\mu_2 k + \sqrt{\mu_1^2 k^2 + \mu_1 \rho_1 \alpha}} \right] + 4\alpha k = 0$$

where μ's are the coefficients of viscosity and other quantities are as previously defined. He has likewise shown that there is one or no positive root according as k is less or greater than

$$\left[\frac{(-g)(\rho_2 - \rho_1)}{T} \right]^{1/2}$$

1.3 Effects Initiating Departure from the Linear Theory

A case of considerable interest arises when we consider the insertion of a layer of fluid of intermediate density at the interface between our two initial fluids. Intuitively one would expect that α would be reduced at the two interfaces which now result, due to the lessening of the density differences at the interfaces. Of even greater interest is the case in which one has a gradually varying density across the interface, as opposed to a true discontinuity. In his Lagrangian treatment of the linear theory of Taylor instability, neglecting surface tension and viscosity, Carter[5] has described the variation of α with thickness of the gradient region, both for a uniform intermediate layer and for a region in which the density variation is exponential in form. In both cases α decreases as the thickness increases. The explicit results for interfaces with which this work is concerned are given in Chapter 4.

It was observed in the experiments of Lewis[6] that the initial sinusoidal disturbance on an air-water interface became asymmetric in its final stages. The form is that of spikes of heavy fluid extending into the light fluid, and rounded regions which may be thought of as bubbles consisting of the lighter fluid rising into the heavier fluid.

Some previous experiments of Davies and Taylor[7] may be invoked to give an a priori estimate of the rate of growth which is to be expected in the asymptotic form. The work of Davies and Taylor showed that large bubbles of air in a liquid have a spherical upper surface and rise at constant velocity V where

$$V = \frac{2}{3}(rg)^{1/2}$$

(see Chapter 3). r is the radius of the surface, and g is the acceleration of gravity. Pennington has shown that for a two-dimensional bubble the rate of rise is also constant, but the constant 2/3 becomes more nearly unity, about 1.1.

The spike of heavy fluid, on the other hand, can be thought of as being in free fall in the acceleration field. The spike will be essentially isolated from the bubbles around it. It will experience a force due to the buoyancy of the lighter fluid and may be acted upon by other hydrodynamic forces. However, in no case will we expect the acceleration of the spike to be larger than g times an Atwood factor, i.e.,

$$a = g\frac{\rho_2 - \rho_1}{\rho_2}$$

where ρ_2 is the density of the heavier fluid.

We see then that the amplitude, A, of the spike should increase as

$$A = A_o + Vt + \frac{1}{2}at^2$$

and that after sufficient time has elapsed the growth may be proportional to t^2, provided we ignore the effect of viscosity of the fluids.

Another effect which, it appears, assumes importance in the growth of the Taylor instability is the so-called Helmholtz instability.[8] This instability arises at an interface when there is relative motion of two fluids in a direction parallel to the interface. It is responsible for the formation of ocean waves, for example.

The condition for Helmholtz instability may be written as

$$V^2 > \frac{\rho + \rho'}{\rho\rho'}\left[\frac{g(\rho - \rho') + K^2T}{k}\right]$$

If the only forces tending to stabilize the interface are those of surface tension, i.e., g = 0, we have, for instability,

$$V^2 > \frac{\rho + \rho'}{\rho\rho'}\,kT$$

Finally, it is expected that in a viscous fluid turbulence will arise when the Reynolds number

$$R = \frac{\rho v \ell}{\mu}$$

becomes of the order of 2000.[9] ρ is the density, v the velocity, and μ the viscosity of the fluid. ℓ is a characteristic length associated with a form moving through the fluid, i.e., the thickness of the boundary layer. We will show later that this effect enters into the experimental observations.

Chapter 2

GENERAL EXPERIMENTAL TECHNIQUES

In order not to interrupt the description of the principal experimental work, it seems proper here to describe briefly the photographic methods used in observing the various phases of the Taylor instability and the means of analysis of the data.

2.1 Photographic Method

The nature of the phenomena being observed usually necessitated the use of photographic equipment capable of time resolution of the order of milliseconds. We used a Kodak high-speed camera, made by Eastman Kodak Co. of Rochester. This camera is a 16 mm framing camera, in which the film runs continuously while the image is tracked on the film by means of a rotating flat-sided prism. The maximum framing rate is nominally 3,000 frames/second, and this framing rate was used for all of our observations. A synchronizing cam is provided on the camera by which arrangement action is begun when a suitable framing rate has been reached. The actual exposure time of the camera is about one-fifth the framing time. Hence at a framing rate of 3,000 frames/second, the exposure time is 1/15,000 second.

To establish an absolute time scale by means of which the velocities and accelerations can be measured, a small argon lamp is provided in the camera near the film gate. This lamp is mounted so as to produce timing marks on the edge of the film. To provide accurate timing marks, a circuit was devised which consisted of a 100 kc crystal oscillator. The frequency of this oscillator was sub-divided by three blocking oscillators to 1 kc. The 1 kc pulses thus produced were used to drive a univibrator which produced output pulses approximately 100 microseconds long, and spaced at 1 millisecond intervals. This circuit was developed by P. W. Byington and is available from the Electronics Group, P-1, of the Los Alamos Scientific Laboratory as Model 110, 1 kc timing pulser.

2.2 Data Analysis

The analysis of the data was necessarily accomplished in several ways. For example, observation of the various pictures as slow motion movies proved useful in aiding qualitative notions of the behavior of the interfacial instability. Enlargement of the photographic negatives to 8-1/2" x 11" size was also of interest in that it permitted detailed study of various phases of the formation of the growth. However, the great bulk of data analysis was done with Leitz Ortholux microscopes at low magnifications (of the order of 20 diameters). By means of the precision stages developed for use in the analysis of nuclear emulsions, measurements could be made of the positions and amplitudes of the various interfaces with reference to certain

fiducial points on the apparatus. The radii of large bubbles and their velocities were similarly measured on the Vickers projection microscope.

In view of the extremely short exposure times of the camera, bright lighting is required to give adequate image density on the film. We used Super-XX film, which has a Weston tungsten rating of 100. Illumination was most satisfactory when the objects being photographed were lighted from the back. Ordinarily, six reflector flood lamps (RFL 2) were used to illuminate a diffusing screen immediately behind the object being photographed. The lens aperture was usually f/5.6. Development of the film in D-76 developer for 12 minutes in a tank or at the rate of 9 feet/min in a developing machine gave adequate image densities.

Chapter 3

TAYLOR INSTABILITY ON THE SURFACES OF LARGE BUBBLES

At the beginning of this work, it was suggested[10] that the upper surface of a bubble of air in water provided the necessary conditions for the Taylor instability. In this system there exists an interface between the light and the heavy fluid in which the equivalent acceleration is directed upward, that is, from the light to the heavy fluid. Under these conditions, and in the absence of appreciable surface tension effects, we should expect to see the development of the Taylor instability on the upper surface of the bubble.

3.1 Apparatus

To observe this phenomenon and to gain experience in high-speed photography, we constructed a tank with Lucite walls. The base of the tank was square, 18 inches on a side, and the height of the tank was 3 feet. As indicated in Fig. 3.1 a rod was mounted horizontally near the bottom of the tank. At the center of the rod was mounted a spun copper hemisphere. A centrally located nozzle at the bottom of the tank enabled the hemisphere to be filled with air. A small motor was attached to the rod so that the hemisphere could be rotated rapidly. In addition, a microswitch was mounted on the shaft of the motor in such a way that the power to the motor was shut off at about the time of release of the bubble.

3.2 Experimental Results

It was our initial intention to produce a bubble by the means described above, and then to perturb the upper air-water interface by means of rods extending across the tank. We found, however, that as the bubble was released from the hemisphere a small spray broke off at the point of contact of the lip of the hemisphere and flew upward inside the bubble, striking the front and upper surfaces. The perturbations thus achieved proved sufficient both in size and interest to cause us to abandon the original plan. The growth of the Taylor instability on a typical bubble is shown in Figs. 3.2 through 3.10.

Subsequent to the initial growth of the instability on the upper surface of the bubble, we observed that the protuberances thus generated tended to wash down and under the bubble, the upper interface finally becoming stable. Apparently the flow pattern established on the upper surface stabilizes that surface.

In their previous work Davies and Taylor[7] had established that bubbles of air rising in nitrobenzene in steady state attained a velocity $v = 2/3\ (rg)^{1/2}$. This relation is derivable on the assumption of potential flow of the fluid about a sphere when one writes Bernoulli's equation for the fluid which is near the tip of the bubble. In the same paper Davies and Taylor

describe their measurements of the pressure distribution about a sphere in a wind tunnel. They found that the pressure distribution was remarkably close to that predicted by the potential theory.

We have been able to extend the measurements of Davies and Taylor to bubbles of larger radii in the present experiment. The radii were measured by recording coordinates of 20 points on the silhouette of the pictures, the observations being made by means of the Vickers projection microscope. A least squares fit was made to two sets of ten points each and the radius taken to be the mean radius derived from these two sets of measurements. The velocity of the bubble was measured at its tip by use of fiducial marks in the picture (Figs. 3.2 through 3.10). Appropriate corrections were made for the parallax resulting from the fact that the bubble and the fiducial marks were not at the same distance from the camera. The measured velocities as a function of radius for several bubbles are shown in Fig. 3.11 along with the previous results of Davies and Taylor. The rms deviation of our points from the line representing $v = (2/3)\ (rg)^{1/2}$ is 3 percent. Our estimated experimental errors were as follows: determination of bubble radius, ± 2 percent; determination of bubble position, ± 2 percent; timing measurements, ± 1 percent. It may be noted that the timing measurements in this series of photographs are considerably less accurate than those in the subsequent series. The reason is that the timing extended over a considerable footage of film and that the crystal-controlled timing marker generator was not available at the time these bubble pictures were made. The timing was therefore based on the 60 cycle line frequency, which drove the argon bulb in the camera. Hence the timing marks were more widely spaced by a factor of about 10 and their beginnings were not as clearly evident as were those produced by the crystal generator.

Chapter 4

THE INSTABILITY OF INTERFACES UNDER UNIFORM ACCELERATION

4.1 Apparatus

After the publication of Sir Geoffrey Taylor's theoretical paper in which Taylor instability was first described, D. L. Lewis[6] observed by experimental means the growth of the instability on interfaces of air-water, as well as on air-benzene and air-glycerin interfaces. We have constructed a machine essentially identical to that of Lewis. Our machine is shown in schematic form in Fig. 4.1.

The Lewis machine consists of a large air reservoir (A), beneath which is fixed a rectangular tube (B) made of Lucite. At the center of the tube is a flange (C), in which is mounted a thin diaphragm. Lewis found it convenient to use shellac diaphragms, but we have had success with glass sheets having thicknesses of the order of 3 to 4 mils. At the bottom of the tube is a foil (D). This foil has sufficient strength to withstand moderate pressures in the pressure vessel.

Air lines are provided both to the upper pressure vessel and to the lower half of the rectangular acceleration tube. Supported on the thin glass diaphragm is a liquid, for example, water; or, more frequently in our experiments, a pair of liquids.

In order to produce an initial disturbance on the surface of the liquid or on the liquid-liquid interface, we have used a cylindrical bob driven by a solenoid. Electrical power to the solenoid is furnished by means of two spark plugs which enter the top lid of the pressure vessel. The driving circuit for the solenoid is described in detail in Appendix A.

In the operation of the Lewis apparatus, the upper and lower pressure chambers are filled. The two pressure chambers are then isolated from each other by the closing of valves on the air lines. When the foil at the bottom of the acceleration tube is ruptured, the unbalanced pressure drives the liquid down the accelerating tube and the instability is observed on the upper interface.

4.2 Experimental Procedure

With Lewis' results as our starting point, we wished to investigate the effects of surface tension and viscosity on the rate of growth of Taylor instability. To be able to observe the instability in more detail, we decided to make use of the density factor to reduce the rate of growth. It was therefore decided to study interfaces of two liquids of densities much more nearly the same than those of water and air. By this choice we were also able to study a greater variation of surface tension than would be possible in the observation of a water-air

interface. Water, n-heptane, isoamyl alcohol, and n-octyl alcohol were the liquids chosen for our observations. The physical properties of these liquids are given in Fig. 4.2. In addition, we lowered the interfacial tension at a water-n-heptane interface by adding a surface active agent (aerosol) to the water. Thus a variation in surface tension of a factor of 20 was obtained while the other properties of the fluids were essentially unchanged. The acceleration, a, of the interface, expressed in units of g, is

$$a = \frac{13.6p}{L}, \text{ where p is the pressure in centimeters of mercury}$$

and h is the equivalent water height of the column in centimeters. The range of accelerations which we studied with the Lewis apparatus was from 20 to 100 g. To cover the region of interest, wavelengths of 2, 4, 7, and 10 mm were chosen. The frequencies necessary to give these wavelengths were calculated from the equation

$$\nu = \left\{ \frac{1}{2\pi} \left[\frac{\lambda^2 g(\rho-\rho') + 4\pi^2 T}{\lambda^3 (\rho + \rho')} \right] \right\}^{1/2}$$

which is that for waves in a fluid with a depth that is large compared to the wavelengths. An effort was made to measure the wavelengths as observed in the initial stages of growth, but in all cases we have used the calculated wavelengths. These calculated wavelengths have been found to be in agreement with the observed values and are considered to be somewhat better values for the wavelengths because of the accurately known frequencies of the oscillator used to drive the transducer.

The densities of the various liquids used in our experimental work were measured with a Westphal balance. With the exception of the isoamyl alcohol, all liquids were Eastman Kodak white label grade. The isoamyl alcohol was Eastman Kodak yellow label, hence of somewhat lesser purity.

All interfacial tensions of interest were measured with a duNoüy tensiometer. This device measures surface tension by the ring method, the force associated with moving the ring through the interface being furnished by a torsion wire. Some of the values for interfacial tensions obtained by this means were not in good agreement with those given in literature. A notable example is that of a water-heptane interface, for which our measured value of the interfacial tension was 39 dynes/cm, whereas the accepted value is 50 dynes/cm. In all cases we have accepted our measured values, acting on the assumption that the liquids used by us probably had various degrees of impurity. It should be pointed out, however, that the ring method for the measurement of interfacial tension has never been proved entirely reliable[11] It may also be noted that, as Pennington[3] has pointed out, the numerical value of the interfacial tension is felt only in the one-fourth power in the rate of growth equation. For this reason discrepancies in our measurements with those of the literature may be discounted to some extent.

4.3 Experimental Results

As discussed in Chapter 1, one of the most important theoretical results of Pennington[3] and of Birkhoff[4] was the prediction of the stabilization of an interface against Taylor instability by the forces of surface tension. In Fig. 4.3 we have plotted the critical wavelength as a function of acceleration for the various interfaces with which we were concerned. In this plot, for a given interface, the region to the right of the curve represents the region of instability, and that to the left represents the region which is stabilized by surface tension. On this same graph we have shown the observed experimental results, differentiating between observations in which the instability was seen and those in which it was not. We observe that in case of a water-n-heptane interface the regions of stability and instability are in quite good agreement with the theory. When the interfacial tension is lowered, through the addition of aerosol to the water, the region of instability is extended to smaller wavelengths for a given acceleration. One observes, however, that an interface of water-isoamyl alcohol appears to be practically uniformly stable, in disagreement with the theory. Our efforts to resolve this anomaly have led to the following explanation.

It is intuitively apparent that the existence of a density gradient at an interface, as opposed to a true density discontinuity, might well lead to inhibition of the Taylor instability. The suggestion of this possibility led to theoretical work by D. S. Carter[5] which showed that this is indeed the case. The effect can be described as a diminution in the exponential coefficient, α, as the region in which the density gradient exists becomes of greater and greater thickness. Carter has calculated the variation in α for various systems of interest. The results of these calculations are shown in Figs. 4.4, 4.5, and 4.6.

To determine whether or not a density gradient existed in the experimental interface of water-isoamyl alcohol, we made use of a schlieren technique. A schematic diagram of the equipment is shown in Fig. 4.7. In a schlieren system a line source of light is placed in the focal plane of a paraboloidal mirror (the mirrors are shown as lenses for greater clarity). The resulting beam of collimated light is directed at a second mirror which brings the beam to a focus. A knife-edge is interposed at the focus of the second mirror, parallel to the image of the line source. Adjacent to the knife-edge is a camera, the focal system of which, together with that of the second mirror, is used to observe an object placed between the two mirrors. The existence of an optical density gradient in the sample being studied will result in the refraction of that portion of the beam passing through the region in which the density gradient exists. Depending on the position of the knife-edge, more or less of the light passing through the refracting region will be admitted to the camera; hence a region of density gradient will appear to have a level of illumination differing from that of the surrounding field. In the diagram an optical wedge which will produce this effect is indicated.

For the purpose of determining the physical existence of a density gradient at a water-isoamyl alcohol interface, we observed by the schlieren technique a cell containing water and isoamyl alcohol. This cell was one of the halves of the acceleration tube used in our Lewis apparatus. The schlieren photographs which resulted are shown as Figs. 4.8, 4.9, and 4.10; these show the progressive thickening in time of the region of optical density gradient. Similar observations on interfaces of water-n-heptane showed only a line at the interface, due to the curvature of the meniscus. An effect similar to that observed with water-isoamyl alcohol was seen to occur at a water-n-octyl alcohol interface. However, the effect was much less pronounced.

According to the theory of the Taylor instability one expects that initially the amplitude of a disturbance grows as cosh αt, where α is a reproduction factor and t is the time. Cosh αt is approximately represented by $e^{\alpha t}/2$, an approximation which becomes increasingly more valid as αt increases. In the later stages of the growth the theory predicts that the lighter fluid will penetrate the heavy fluid at constant velocity, in analogy with the constant rate of rise of bubbles, while the heavier fluid will be in free fall under an acceleration which is constant, but may be diluted by an Atwood factor.[12] Hence one would expect the amplitude to increase according to a form such as $a = a_o + vt + 1/2\ at^2$. In very late stages the term t^2 should predominate and one would expect that the amplitude would be simply proportional to t^2 To check these predictions, we have measured the amplitude of disturbances of various wavelengths as a function of the time. These measurements were made primarily from the 16-mm negatives by means of Leitz Ortholux microscopes at low magnifications. At the same time the estimated mean position of the interface was measured so that the acceleration could be determined. The results of a typical set of such measurements are shown in Figs. 4.11, 4.12, and 4.13. In Fig. 4.11 we have plotted the square root of the observed mean displacement of the interface against the time. The result is a straight line, the slope of which measures the acceleration. The intercept on the time axis indicates the time at which the acceleration began on the arbitrary time scale. Taking the time zero thus obtained as the true zero in time, we have plotted in Fig. 4.12 lnA vs true time. We observe that, while the scatter of the points is considerable, a straight line can be drawn reasonably well through the first portion of the curve. The slope of this line is a measure of the α which is observed experimentally.

In Fig. 4.13 $A^{1/2}$ vs t is plotted for a typical observation. It is seen that in the latter stages of the growth a linear relation applies between these two variables. The slope of the line in this region is a measure of the acceleration of the heavier fluid into the light. Table 4.2b gives a comparison of the observed values of α with those predicted by the linear theory of Taylor and that of Pennington, which has taken into account the effects of surface tension

and viscosity. It is noteworthy that in all cases that α's that are observed experimentally are smaller than those predicted by either of the theories. The probable explanation of this fact lies in the neglect of the mass motion in the theories, since the effect of the term in Bernoulli's equation containing v^2 is assumed to be negligible. Figs. 4.14 through 4.19 show the progressive growth of a disturbance on a water-n-heptane interface.

4.4 Theoretical Implications

Qualitatively one can divide the growth of a disturbance in Taylor instability into four categories. The first of these is to a considerable extent described by the theories of Taylor, Pennington, and Birkhoff. The increase in amplitude is essentially exponential, though with a somewhat smaller α value than that predicted by the theories. If the initial disturbance is sinusoidal, the interface retains its symmetric character about the main displacement axis.

The second phase of the growth may be described as the development of an asymmetry in the interface in which the heavy fluid begins to be constricted, tending toward the formation of spikes, while the lighter fluid tends to bulge in the direction of bubble formation. It seems reasonable that the development of the asymmetry is caused by the dynamic pressure change resulting from the mass motion. For if the fluid particles were constrained to move as predicted by the theories which have so far been offered, the term in v^2 in Bernoulli's equation would set up a pressure gradient across the interface in a direction to cause bulging of light fluid into the heavy. It is clear also that the extent to which this asymmetry develops will depend on the difference in density of the two fluids. If the difference is very great, as for example in an air-water interface, one would expect the constriction of the heavy fluid to be comparatively severe. For liquid-liquid interfaces such as those which have been studied here, in which the density difference is comparatively slight, the degree of asymmetry should be less, and this is experimentally observed to be the case.

In the third phase one observes a mushrooming of the interface. It seems reasonable to ascribe this effect to the Helmholtz instability, in view of the fact that the necessary velocities for the production of Helmholtz instability are present. Experimentally one also observes a distinct variation in the mushrooming effect between interfaces of high and low interfacial tension. The fourth and final phase of the growth may be described as turbulent mixing. Experimental evidence[9] is available to support the notion that turbulence will arise, in general, when the Reynolds number is of the order of 2000. Once again the velocities required to give this Reynolds number are of the proper order of magnitude to make this a reasonable conclusion.

After turbulent mixing has begun, the situation may be described roughly as that which applies in the case of an extensive density gradient. Hence one might say that the effect of Taylor instability is in a sense self-limiting, since the normal course of events leads to a situation in which α is reduced by the formation of a region of density gradient.

Chapter 5

INSTABILITY OF INTERFACES UNDER IMPULSIVE ACCELERATION

5.1 Introduction

A third group of experiments was performed to investigate the effect of impulsive accelerations upon an interface. Three phenomena seem to be of interest: the total growth of an initial interfacial wave due to impulse, the generation of spontaneous waves from minute perturbations, and the change caused by altering the impulse time for a given total impulse. Quantitative results have been obtained for the first two phenomena.

5.2 Apparatus

A sketch of the apparatus is shown in Fig. 5.1. The operational sequence is begun by turning on the high speed viewing camera (not shown). When the camera reaches an appropriate speed the upper mass is released from its solenoid support and then, guided by the vertical guides, it falls freely. Just before the upper mass strikes the lower cell, which contains the fluids under study, it shutters a photocell system which releases the lower frame. Impact of the upper mass upon the lower provides the impulse. The surfaces of impact are made of hardened steel for the purpose of obtaining a short impulse. Average accelerations of the order of 200-300 g over a millisecond interval are obtained.

During the experiments several limitations of the apparatus became apparent. The transparent faces of the cell containing the fluids were made of Plexiglas and even with plates as thick as 3/4 in., it was found that the hydrostatic pressure developed caused distortion of the sides. This has the effect of making the acceleration and pressure oscillatory.

A second limitation is imposed by the camera. It would be desirable to have a time resolution from 5 to 10 times as fast as with our Eastman camera. The Eastman camera frames about 3,000 pictures per second, which means that 2 to 3 frames are obtained for each impulse; hardly enough for detailed wave growth studies. A faster camera, besides allowing a more detailed investigation, might reduce the significance of fluid oscillations. In spite of these difficulties, it is possible to study the total change in the amplitude of an initial wave and it is also possible to observe the appearance of spontaneous waves generated by the impulse.

5.3 Initial Wave Studies

If the impulse were of the form of a constant acceleration over the impulse interval it would be expected that the growth of initial waves would obey the cosh αt law as long as $\eta << \lambda$; that is, if Δt is the time interval and α the growth constant associated with the particular acceleration, then

$$\eta/\eta_0 = \cosh \alpha \Delta t, \text{ where } \eta$$

is wave amplitude and η_0 is the initial amplitude.

The average acceleration can be obtained from the change in velocity of the cell and from a knowledge of the impulse time. Measurement of change of velocity presents no particular difficulty. However, the impulse time is not easy to measure exactly.

The time was estimated by utilizing two different observations. First, the time of contact of the two frames was determined by an electrical method. The electrical signal was displayed upon a dual beam oscilloscope along with a calibrating signal and was photographed. The contact time was measured to be 1.1 millisecond, with a standard error of the order of 0.05 millisecond. Next, the position in laboratory coordinates of both the cell and the liquid interface was determined for each film frame. It was found that the cell changes velocity abruptly (relative to our time resolution), but the change in interface velocity takes place within about 1.1 milliseconds, when 3/4 in. plastic plates are used as cell walls.

Both of these measurements give upper limits on the impulse time, but the actual time is probably not more than 20 percent smaller. Therefore, for cells with 3/4 in. plates, 1 ± 0.1 millisecond was somewhat arbitrarily taken as impulse time. The impulse time for cells with 1/4 in. plates used in some early experiments appears to be 1.7 ± 0.15 milliseconds.

From a knowledge of the acceleration, α may be calculated according to the Pennington theory, and the expected ratio of the wave amplitude after impulse to that before impulse can be determined. These ratios, together with measured ratios, are given in Fig. 5.3. The formula used for the calculation of α included surface tension but not viscosity. This method of analysis assumes that it is permissible to average linearly over oscillatory effects. Because of the nonlinear nature of the phenomenon, this assumption cannot be correct.

Measurements of the natural frequency of the main parts of the cell indicate that the actual impulse resembles the peaked form shown in Fig. 5.4A. The effect of peaks is to lower the growth below that expected from an equivalent rectangular impulse. Viscosity influences the growth in the same direction and it is therefore reasonable to expect smaller wave growths than predicted from theory which is based on an average acceleration and which neglects viscosity. That this does not appear to be the case in our experiments remains an unresolved, but not surprising, problem. As a whole, our results are consistent with expectations and the deviations may well be due to spurious effects associated with the apparatus.

That a peaked impulse gives rise to smaller growth than an equivalent rectangular impulse can be explained as follows:

Consider a peaked impulse of the form shown in Fig. 5.4B as an approximation to the actual case. It may be assumed that the integrated effect (momentum change or area in the figure) and the outer limits of the impulse (Δt_2) are fairly accurately known, but that the

relative heights of the two rectangular portions are not known. Therefore, it is desired to discover the effect of altering the relative heights of the rectangular portions.

First, in a qualitative manner, consider the effect of the two rectangular portions separately as indicated by the shading. If the two portions are considered as separable and the larger portion is assumed fixed, then only the growth resulting from one portion need be discussed, the other being entirely comparable. Now $\alpha \sim \sqrt{g}$, approximately, where g is acceleration. And for a given impulsive momentum change, i.e., a given shaded area in the figure, $g \sim 1/t$.

Thus $\alpha \sim \sqrt{1/t}$ and $\alpha t \sim \sqrt{t}$.

Using these last proportionalities, the expression for η_2, the growth associated with the small portion, may be written as

$$\eta_2 = \eta_o \cosh \alpha_1 \sqrt{\Delta t_1 \Delta t_2} + \frac{\eta_o}{\alpha_1} \sqrt{\frac{\Delta t_2}{\Delta t_1}} \sinh \alpha_1 \sqrt{\Delta t_1 \Delta t_2}$$

where α_1 is the α required by the given momentum change when $\Delta t_2 = \Delta t_1$. Evidently for a fixed $\alpha_1 \cdot \Delta t_1$, η_2 will contribute most when Δt_2 is as large as possible, that is, when $\Delta t_2 = \Delta t_1$. Thus there will be the greatest growth when the total impulse is in the form of a single rectangle.

The above argument must be accepted only in a loose qualitative way since it depends implicitly upon the principle of superposition which is not at all valid for hyperbolic phenomena. An appreciation of magnitudes may be obtained through use of a specific example.

Consider an impulse composed of three joining rectangular portions as shown in Fig. 5.7C. Let the first and last portions have an α of 200 sec^{-1} and a duration of 3/8 millisecond each. Let the central portion have an α of 600 sec^{-1} and a duration of 1/4 millisecond. These values are of the same order of magnitude as those in our experiments.

By successively applying the formulas

$$\eta = \eta_o \cosh \alpha t + (\dot{\eta}_o/\alpha) \sinh \alpha t$$

$$\dot{\eta} = \eta_o \alpha \sinh \alpha t + \dot{\eta}_o \cosh \alpha t$$

to the three sections, the final η may be obtained. It turns out to be $(1.057)\eta_o$. However, if the α values are averaged and the average applied for the whole impulse time, $\eta_{av} = (1.081)\eta_o$. Also if an RMS value of α is taken for the whole impulse, $\eta_{RMS} = (1.10)\eta_o$. (Taking an RMS value for α corresponds to averaging the accelerations associated with the various α values and closely resembles what was actually done in our experimental analysis.) The discrepancy from η of η_{av} and η_{RMS} is about 2.3 and 4 percent, respectively.

5.4 Spontaneous Waves

It is found that impulsive accelerations of the order of 200 g for 1 millisecond do indeed give rise with our apparatus to waves or spikes regardless of the presence of an initial wave. The spikes observed were of heavy liquid protruding into the light; no definite wave crests of the light fluid into the heavy were seen, though it is not certain that they could be resolved with our system even if present. The spikes seem to be randomly placed on the two dimensional interface. An effective "wavelength" could, however, be measured whenever a number of spikes were grouped together. The results of these measurements are given in Fig. 5.3 together with the wavelength of the "most dangerous frequency" of Pennington. This wavelength is that which corresponds to the maximum of the α vs wave number curve. The wave number of the wavelength is given by Pennington as $(a\Delta\rho/3T)$ where a is the acceleration, $\Delta\rho$ the difference in the densities of the two liquids, and T the interfacial tension.

Figure 5.5 shows a plot of the growth of these spikes for an experiment in impulsive acceleration in which spontaneous spikes are observed.

The details of growth are hard to discover because of the poor time resolution of our camera, but some idea of the maximum velocity attained can be acquired.

It was immediately apparent from the pictures of the interface that some sort of oscillation took place, for after the initial impact and the spike formation, cavitation bubbles occurred within the aqueous fluid and within the spikes themselves. To investigate the nature of these vibrations the filled cell was caused to resonate by tapping it at various places, and the audible vibration was recorded by means of a microphone and an oscilloscope. The cell has a dominant vibration at about 1.1 kc/s which appears to be associated with a transverse vibration of the side plates. A cycle of such a wave is shown in the spike growth curve. Evidently, if this wave represents hydrostatic pressure, the observed cavitation would not be surprising.

In runs K-5 and K-6 the camera happened to be so timed with the impact that growth before cavitation was observed. In run L-2 the timing of the camera was slightly different and no growth before cavitation was recorded; however, the initial part of the growth after cavitation was recorded. The first measurable velocity following cavitation for L-2 is actually greater than the cell velocity, but it soon drops off to a lower value. Pictures of an interface under impulse are shown in Figs. 5.6 and 5.7.

It is possible to express the initial amplitude of a wave in terms of its velocity and amplitude at a given time, beginning with the fundamental relations $\eta = \eta_o \cosh \alpha t$ and $\dot{\eta} = \alpha \eta_o \sinh \alpha t$. Thus, $\eta_o^2 = \eta^2 - (\dot{\eta}^2/\alpha^2)$. It was thought an idea of the initial amplitude could be obtained by using the α calculated from the formula involving surface tension, but not viscosity, and choosing the first value of η where $\dot{\eta}$ can be measured with reasonable certainty. However, in each of the cases where spikes possible of measurement are formed, this

procedure gives an imaginary initial amplitude. This result indicates that either the initial velocity is not zero--as indeed it might not be because of cavitation and oscillation effects--or else that for the spikes the Taylor growth law is not valid over the whole of the impulse. Irrelevance of the Taylor theory is quite reasonable since the theory is derived on the assumption that $\eta << \lambda$. This assumption is no longer valid almost as soon as the spikes become perceptible. It appears then, that Taylor instability is responsible for the initiation of the spike, but in our experiments it is not in control of their subsequent development.

5.5 Effect of Impulse Time for a Constant Impulse

Although we have no quantitative experimental results, it seems worth while to point out what is involved in variable impulse time. Consider again the basic growth equation, $\eta = \eta_0 \cosh \alpha t$. The quantity α is presumably roughly proportional to the square root of acceleration. On the other hand the acceleration for a given impulse (i.e., given momentum change) is proportional to 1/t, thus, αt is approximately proportional to $\sqrt{t}$ and for two different impulse times (but the same momentum change),

$\alpha_2 t_2 \cong \alpha_1 \sqrt{t_1 t_2}$. Thus, $\eta_2 \cong \eta_0 \cosh \alpha_1 \sqrt{t_1 t_2} = \eta_0 \cosh (\text{const} \sqrt{t_2})$.

This gives an idea of what might be expected as the impulse time is shortened; in the limit, as t_2 approaches zero, no growth would be expected of an initial wave and, consequently, spikes arising from small perturbations should not appear.

In an attempt to shorten the impulse time through the use of explosives, a cell similar to the one used in the previous apparatus was accelerated by a rocket jet obtained from high explosives. However, the cell was not sufficiently rigid and spread the duration of the impulse to more than a millisecond. It might be possible to eliminate this difficulty through increased cell rigidity and careful design.

5.6 Conclusions

Because of the complicated and unknown mixing of various phenomena (e.g., vibration, cavitations, shock waves) and because of the limited extent of the experiments, our results for impulsive accelerations should be taken only as indicative. The results of our observations follow. During impulse, initial waves grow as predicted by the theories of Taylor, Pennington, Birkhoff; spikes which often arise correspond to the most dangerous wavelength of Pennington; and the rate of growth of spontaneous spikes does not appear to correspond to the Taylor theory.

In future experiments in impulsive acceleration, particular care should be exercised in the design of the cell to eliminate low-frequency, high-amplitude vibration. In addition, the camera framing speed should be increased to about 30,000 frames per second for viewing millisecond impulses.

REFERENCES

1. Leigh Page, Introduction to Theoretical Physics, D. Van Nostrand Co., second edition, page 254, 1949.
2. Sir Geoffrey Taylor, Proc. Roy. Soc. (London) A201, 192 (1950).
3. R. H. Pennington and R. Bellman, Princeton University Report, Project Matterhorn January 28, 1952.
4. G. D. Birkhoff and R. Ingraham, Harvard University Report, December, 1952.
5. D. S. Carter, unpublished work.
6. D. J. Lewis, Proc. Roy. Soc. (London) A202, 81 (1950).
7. R. M. Davies and Sir. G. Taylor, Proc. Roy. Soc. (London) A200, 375 (1950).
8. See, for example, L. M. Milne-Thompson, Theoretical Hydrodynamics, The MacMillan Company, New York, page 374, 1950.
9. B. A. Bakhmeteff, The Mechanics of Turbulent Flow, Princeton University Press, Princeton, page 13, 1941.
10. C. Longmire, private communication.
11. W. D. Harkins, "Determination of Surface and Interfacial Tension," Physical Methods of Organic Chemistry, Arnold Weissberger, editor, Interscience Publishers, New York, 1945.
12. E. Fermi and J. Von Neumann, Los Alamos Unclassified Report TM-106, August 19, 1953.

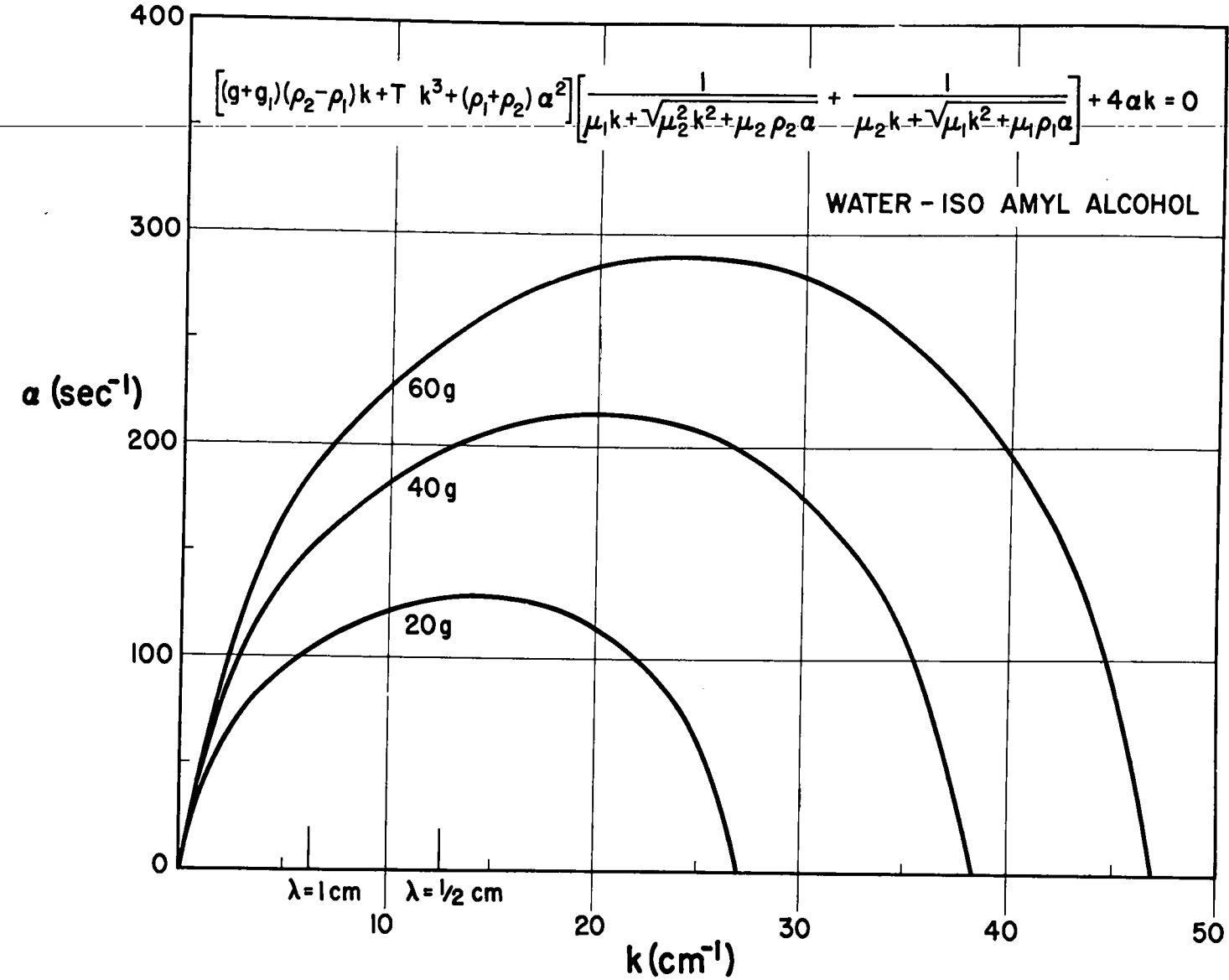

Fig. 1.1. α vs wave number. Calculated from Pennington's results.

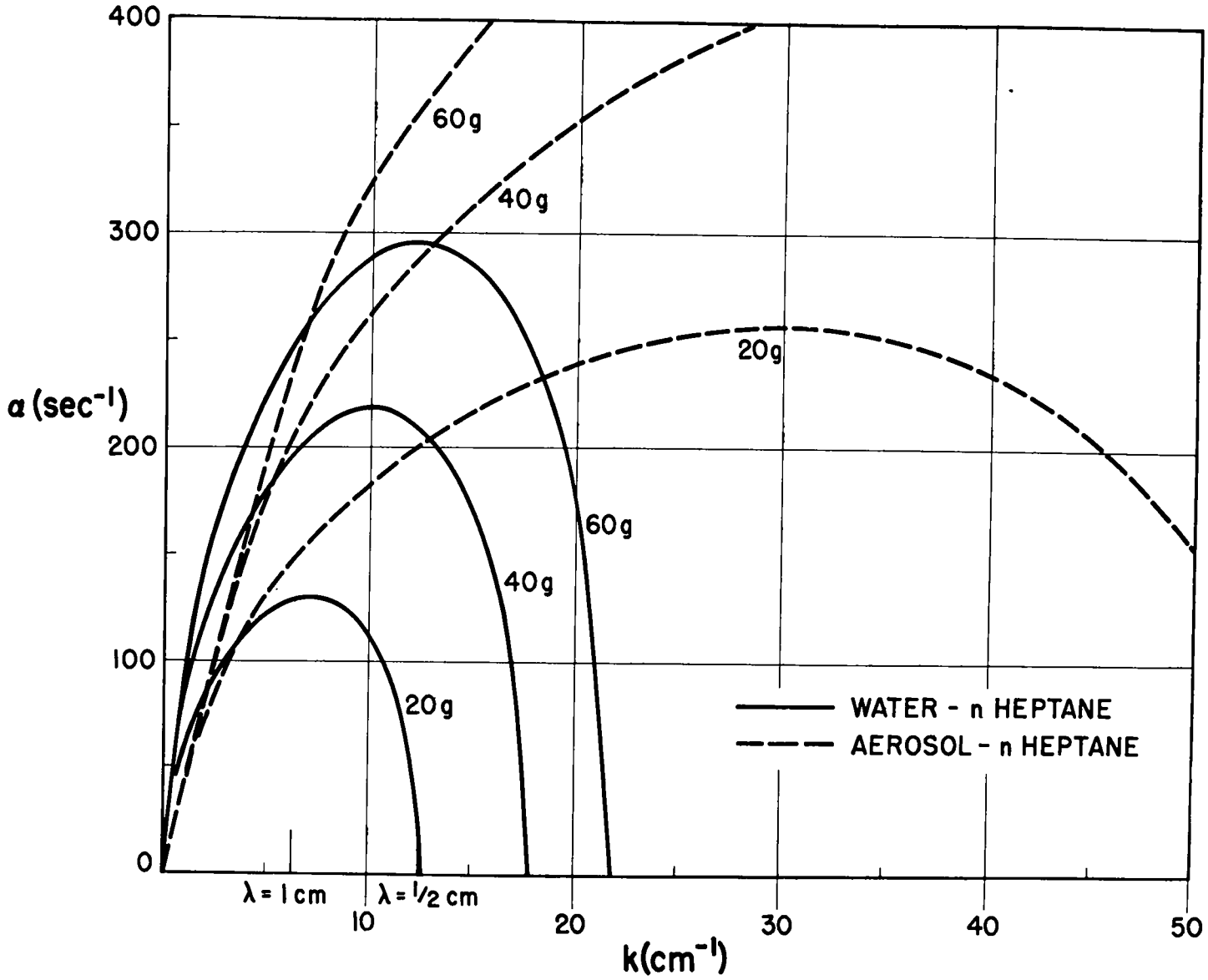

Fig. 1.2. α vs wave number. Calculated from Pennington's results.

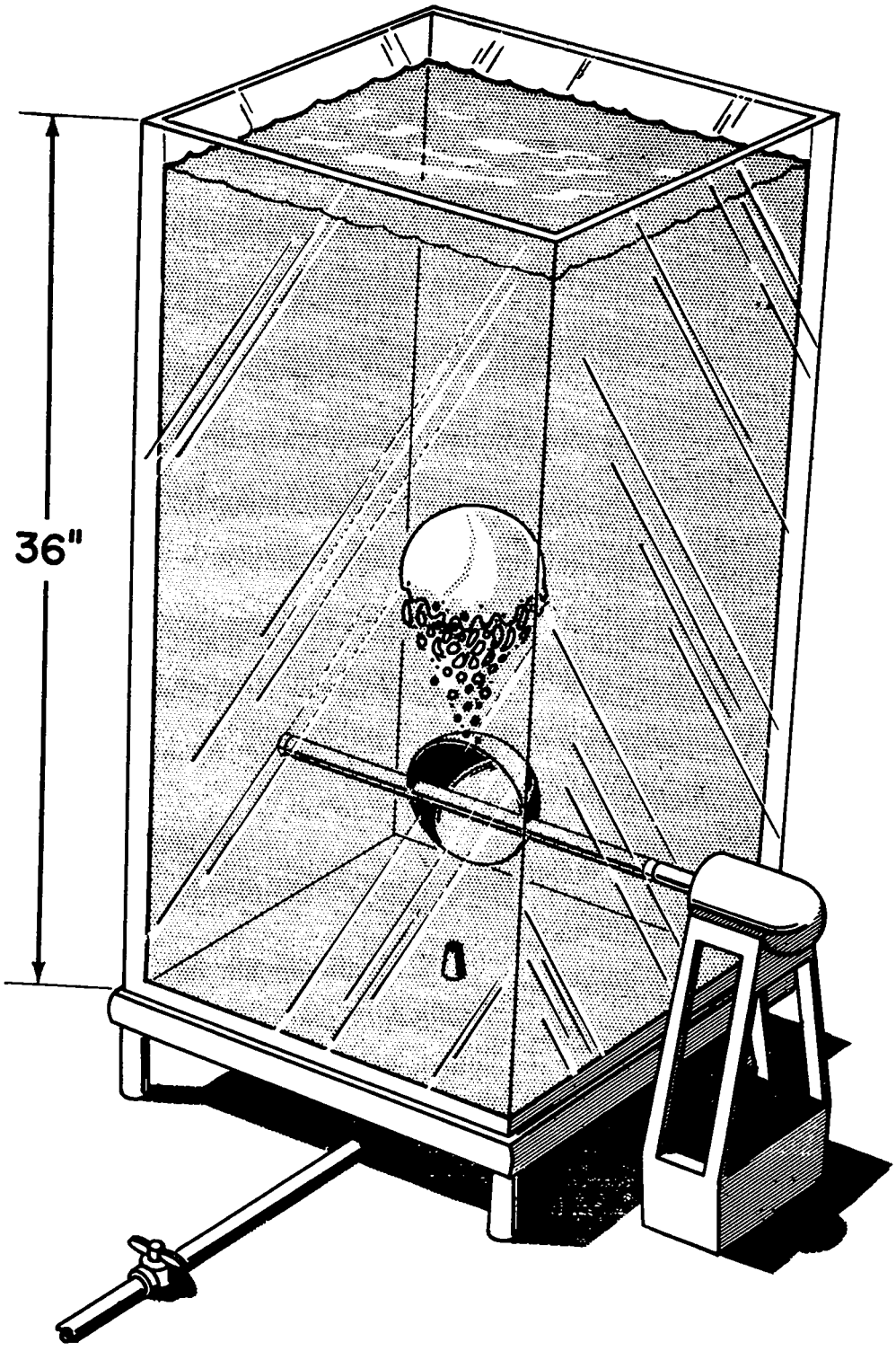

Fig. 3.1. Bubble tank.

Figs. 3.2 through 3.10

Development of Taylor instability on the upper surface of an air bubble in water. With an arbitrary time zero, the pictures are taken at the following times (milliseconds): t = 0, 16.7, 25.0, 33.3, 50.0, 58.3, 66.7, 83.3, 125.0. The horizontal grid in the background has a spacing of 2 inches.

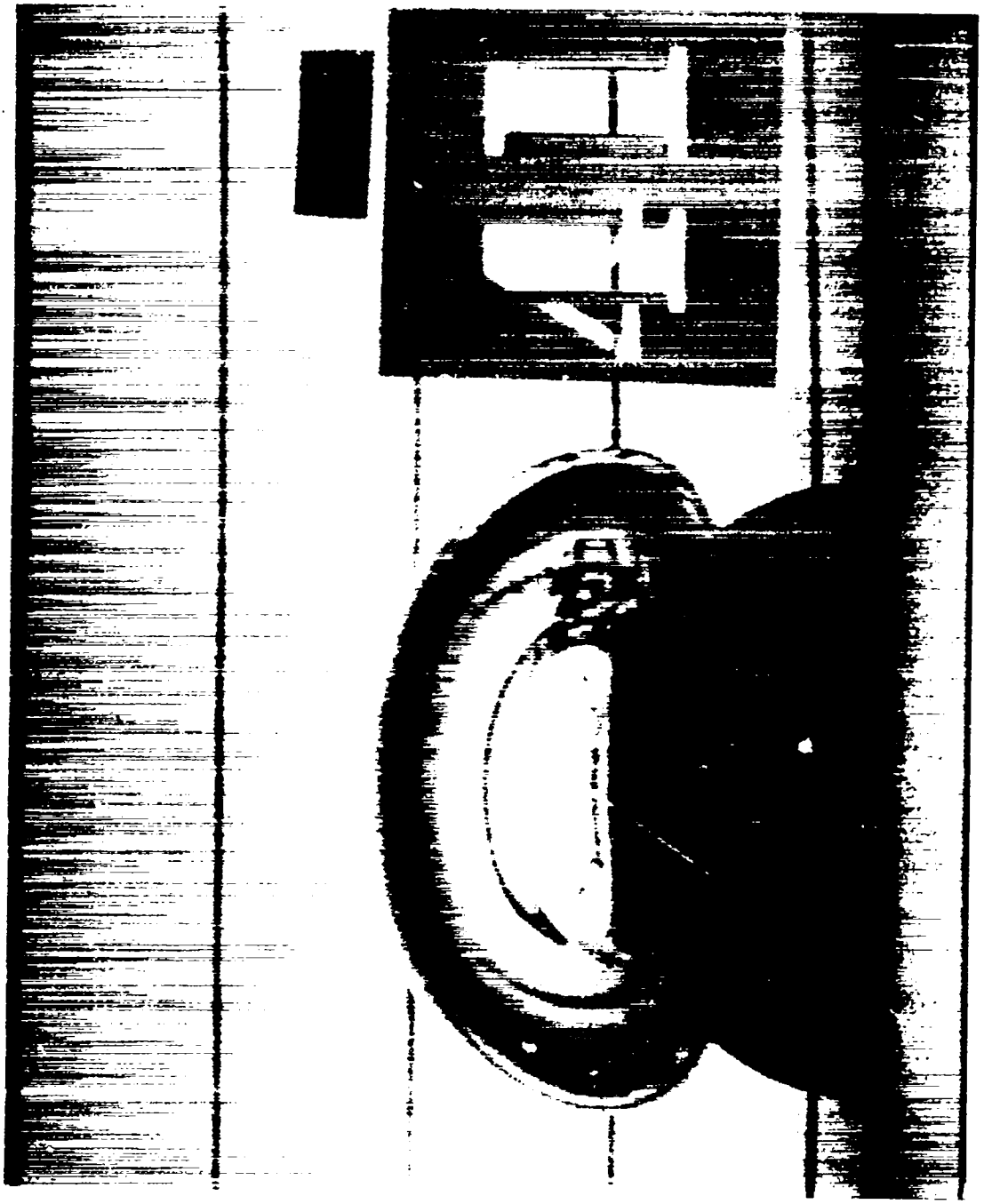

Fig. 3.2

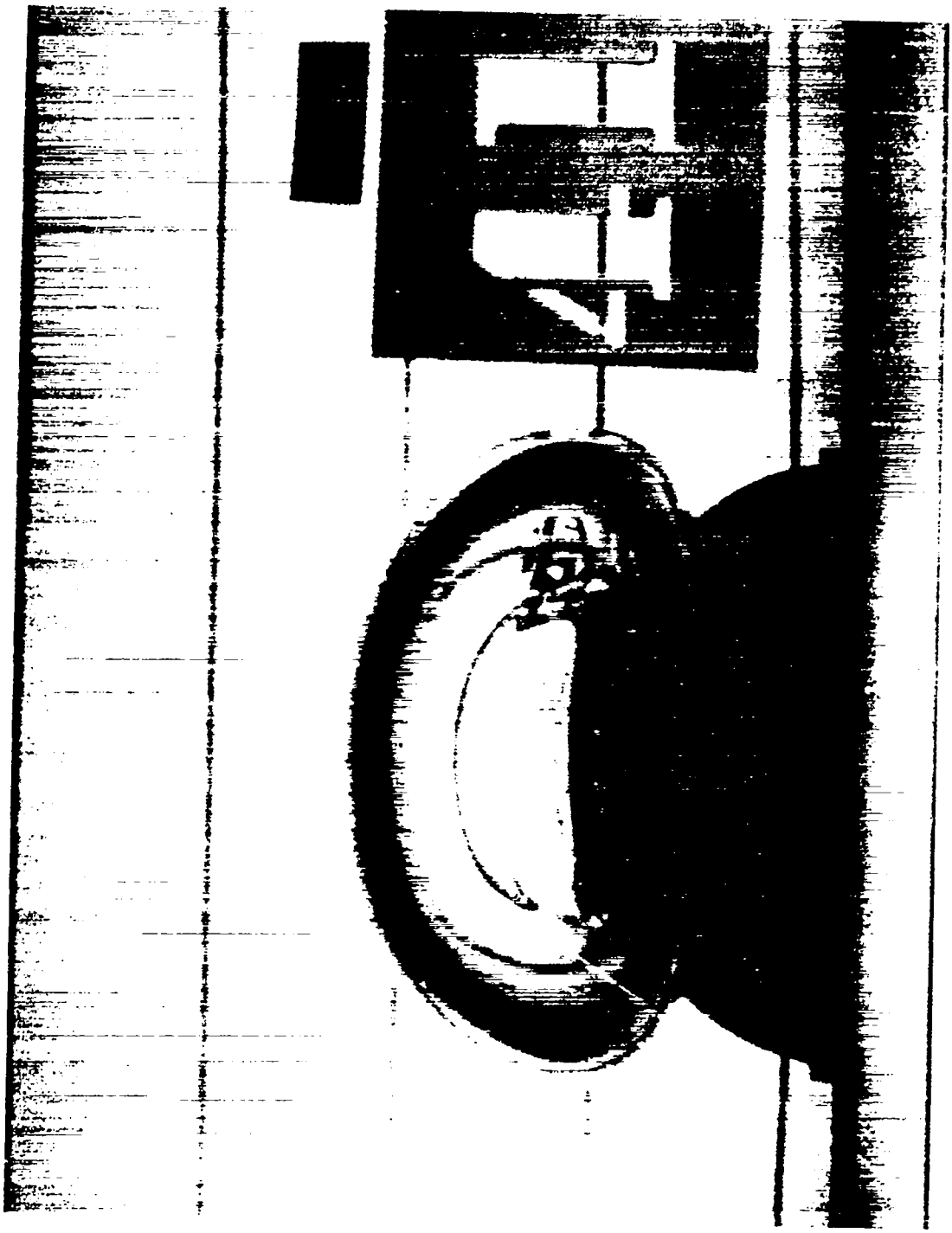

Fig. 3.3

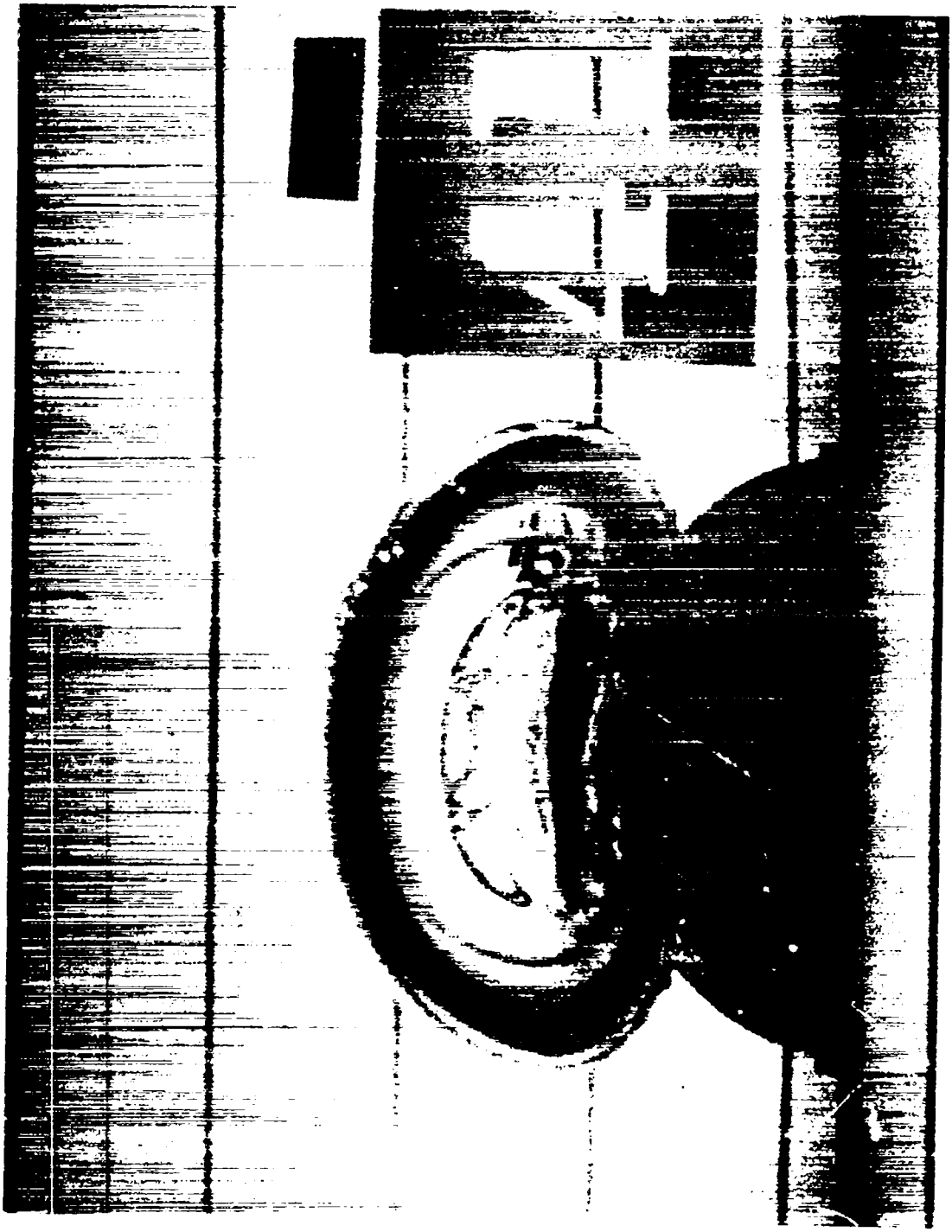

Fig. 3.4

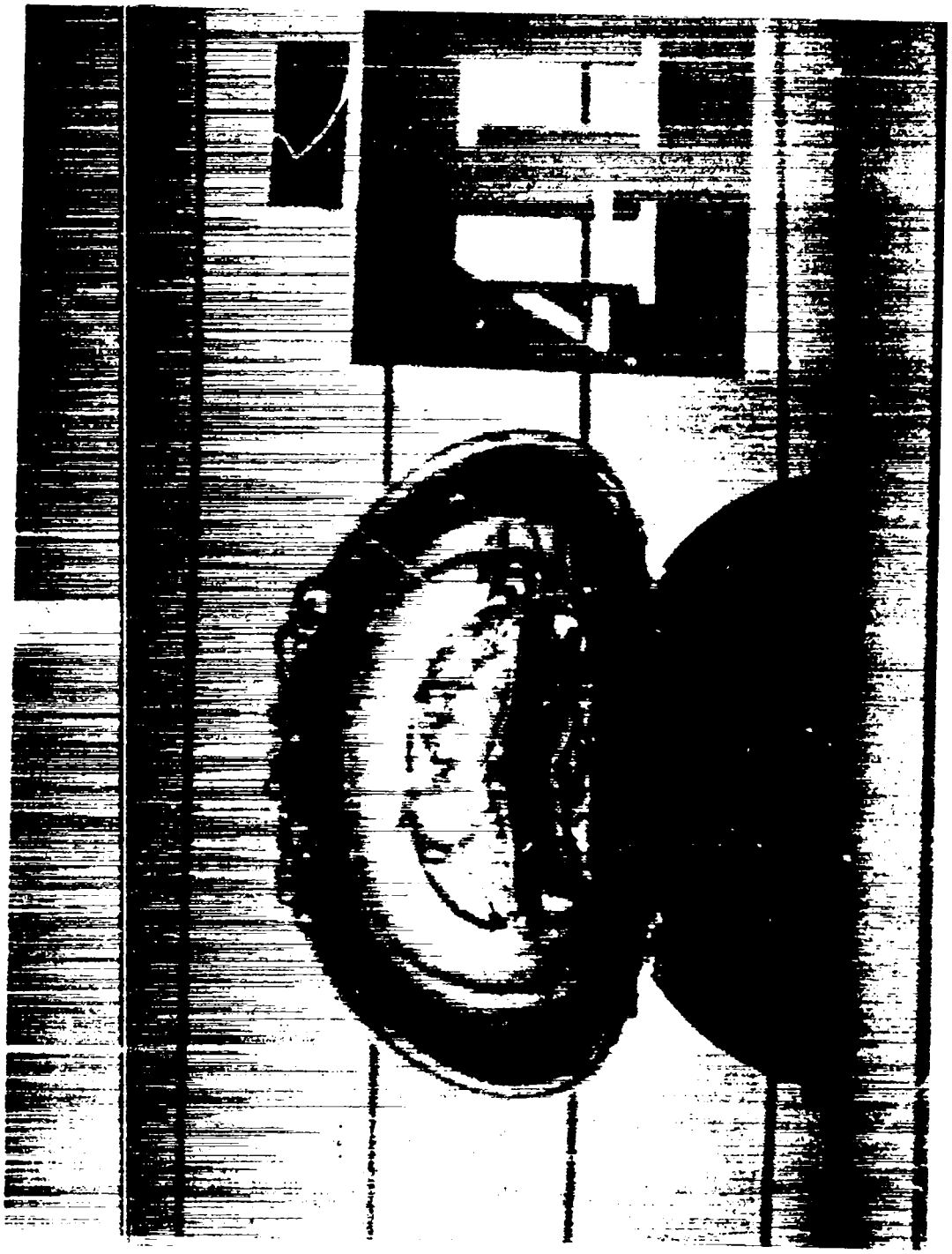

Fig. 3.5

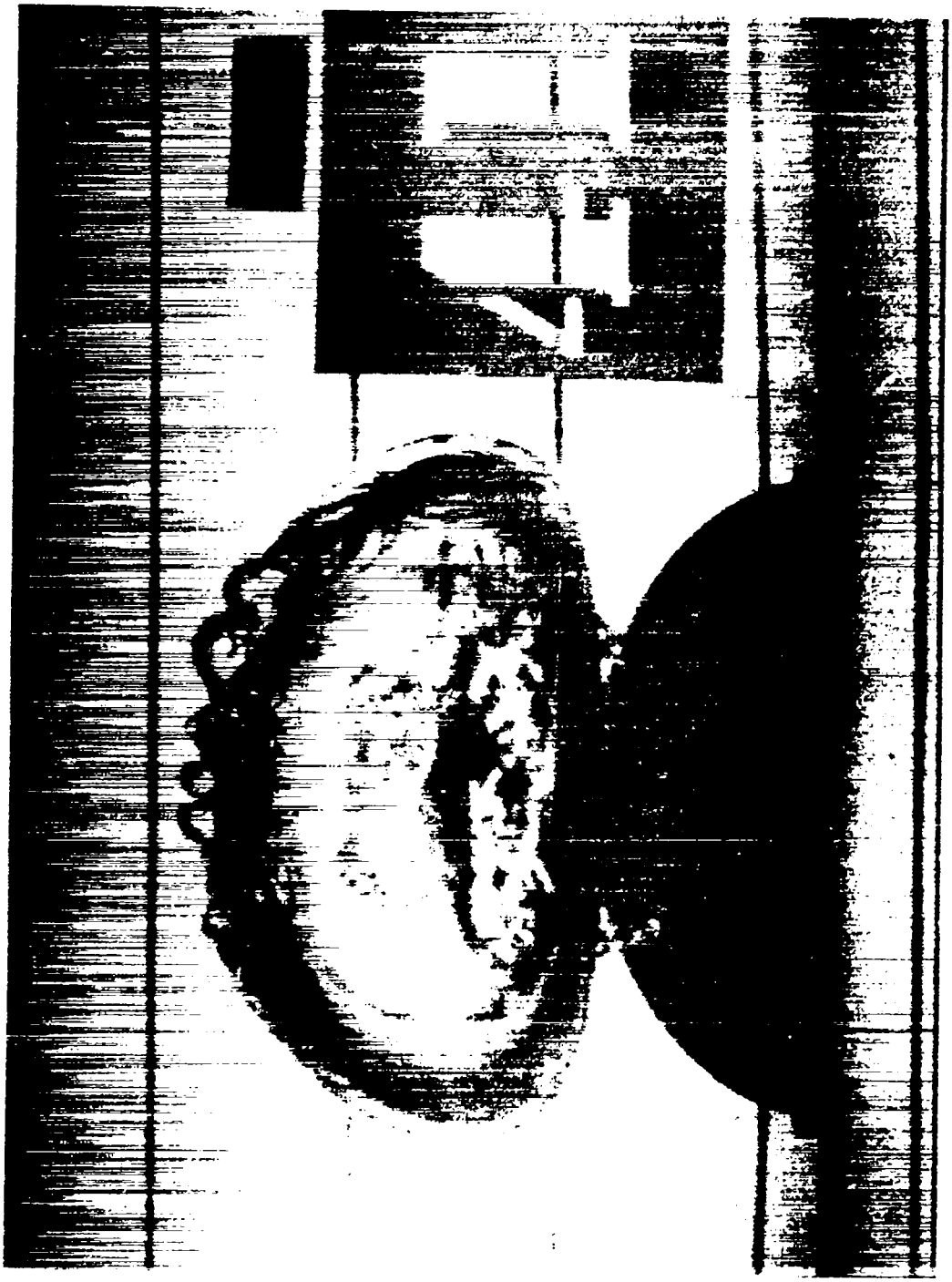

Fig. 3.6

Fig. 3.7

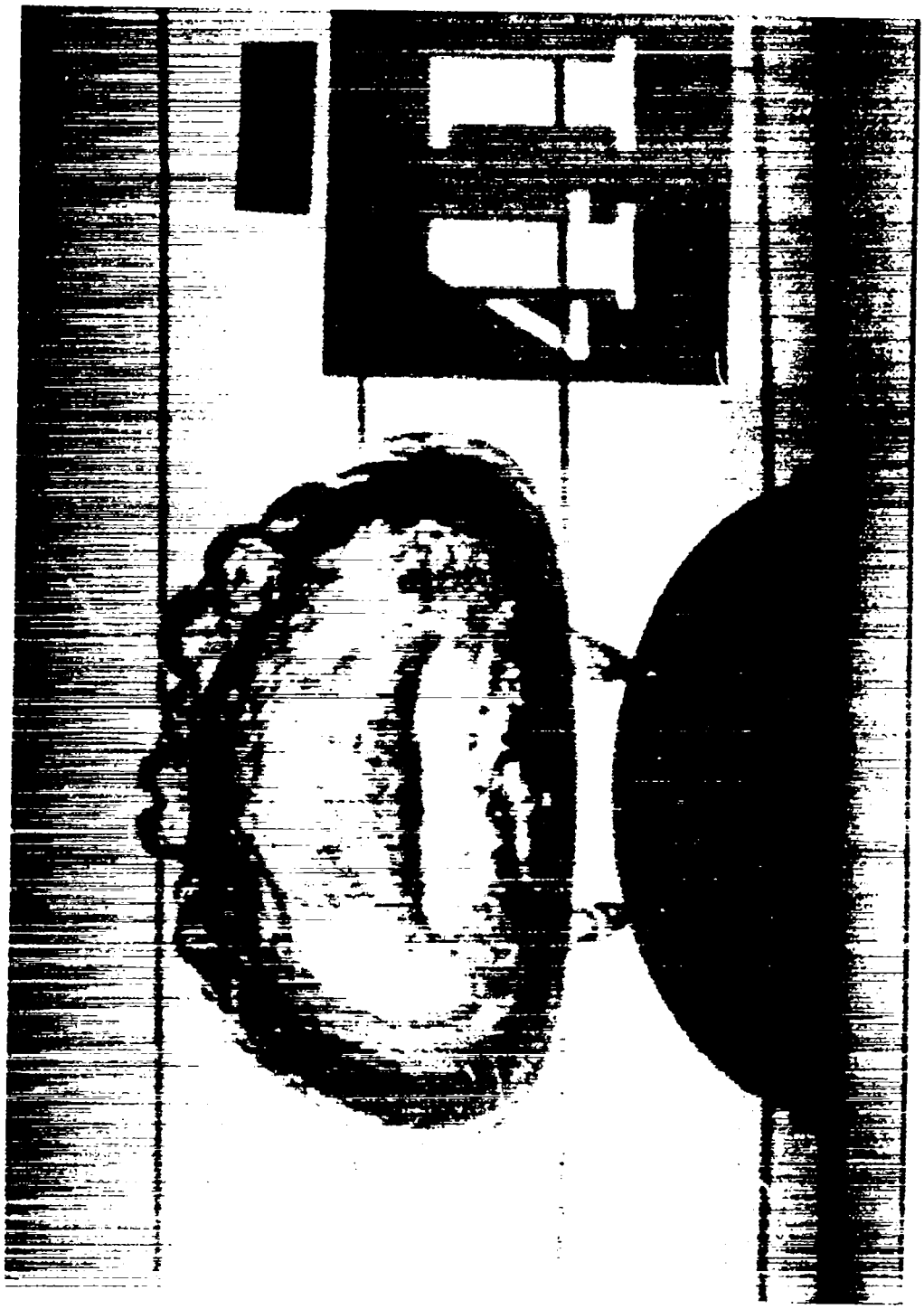

Fig. 3.8

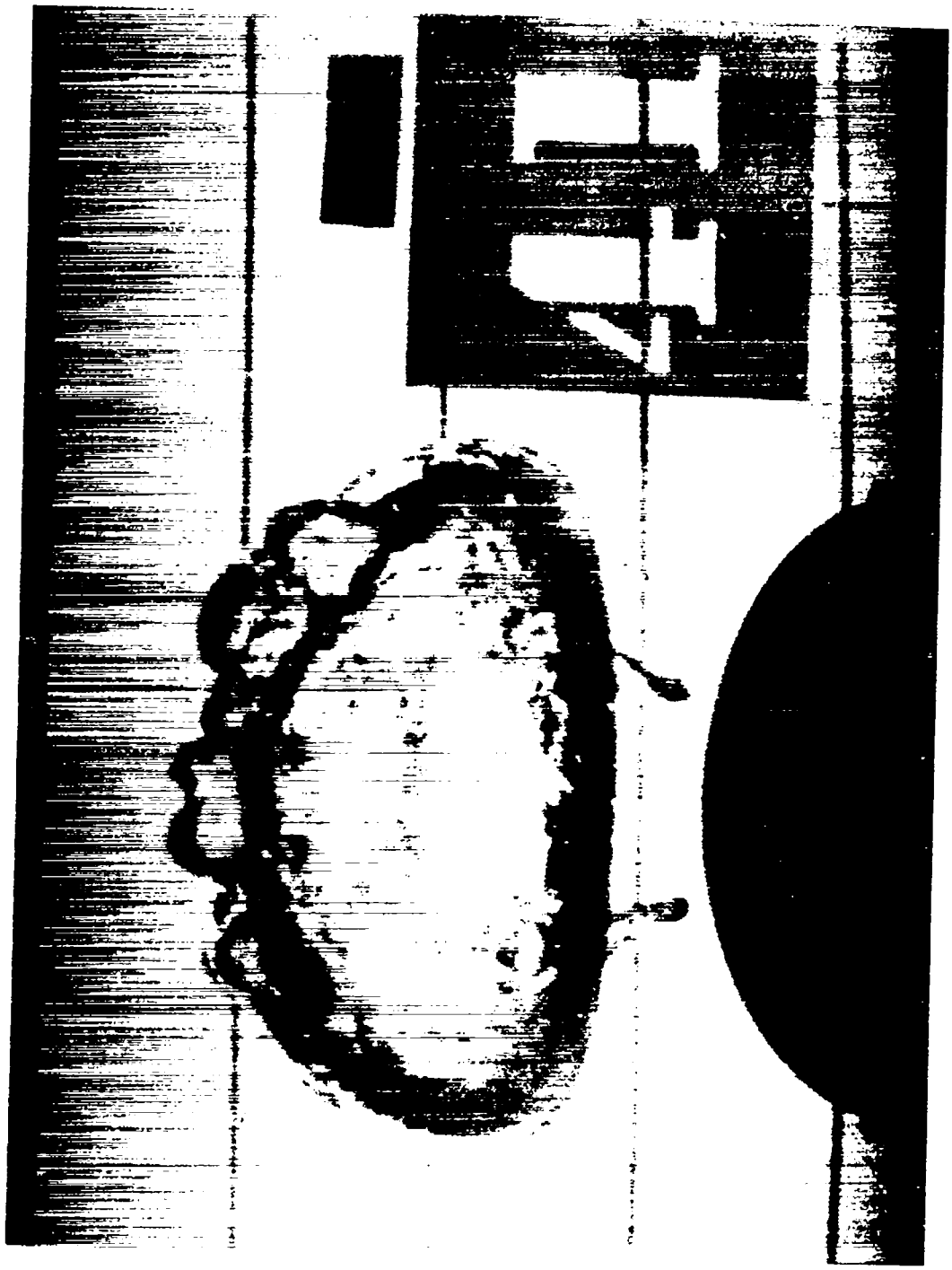

Fig. 3.9

Fig. 3.10

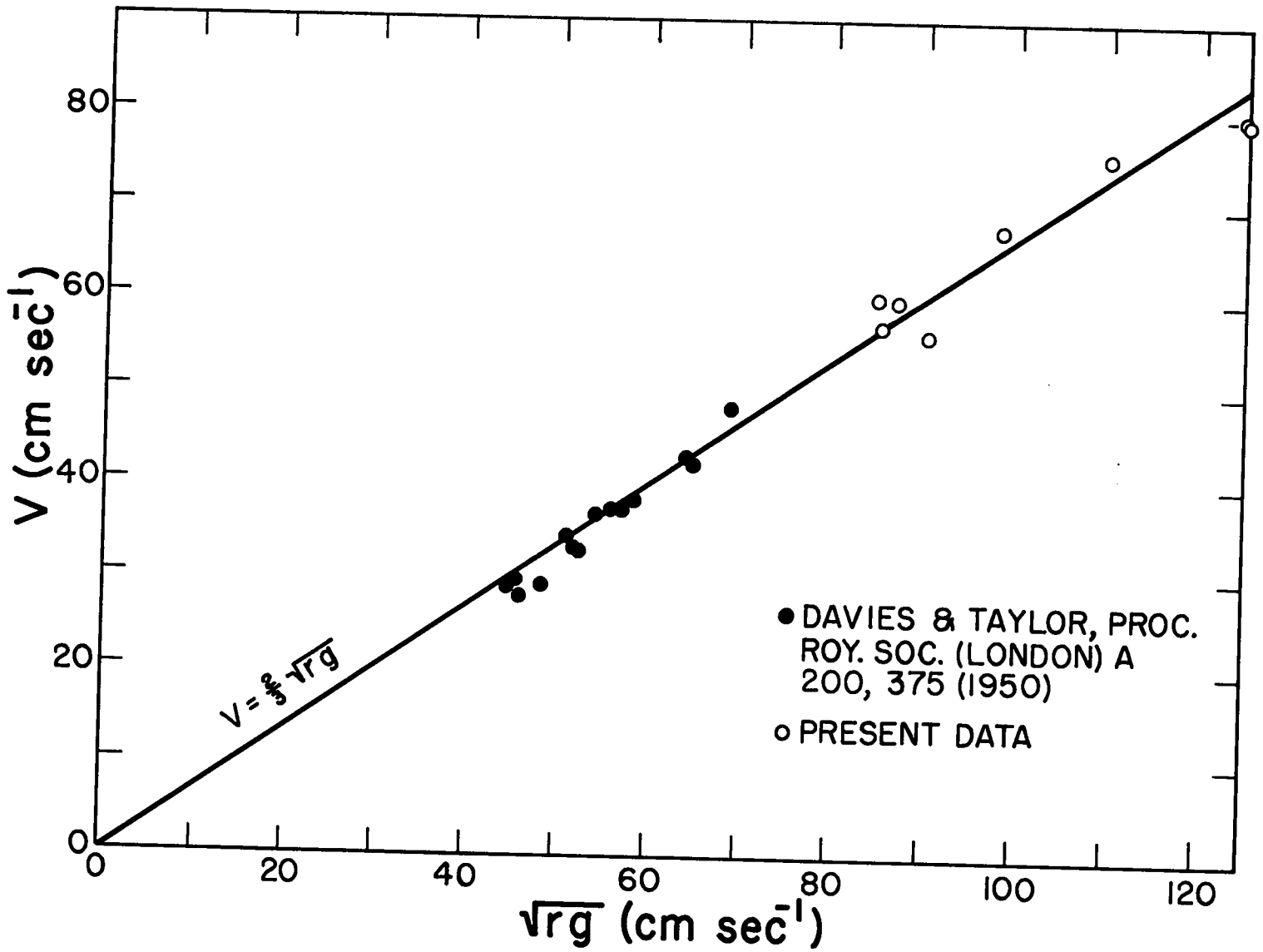

Fig. 3.11. Bubble velocity vs $(rg)^{1/2}$

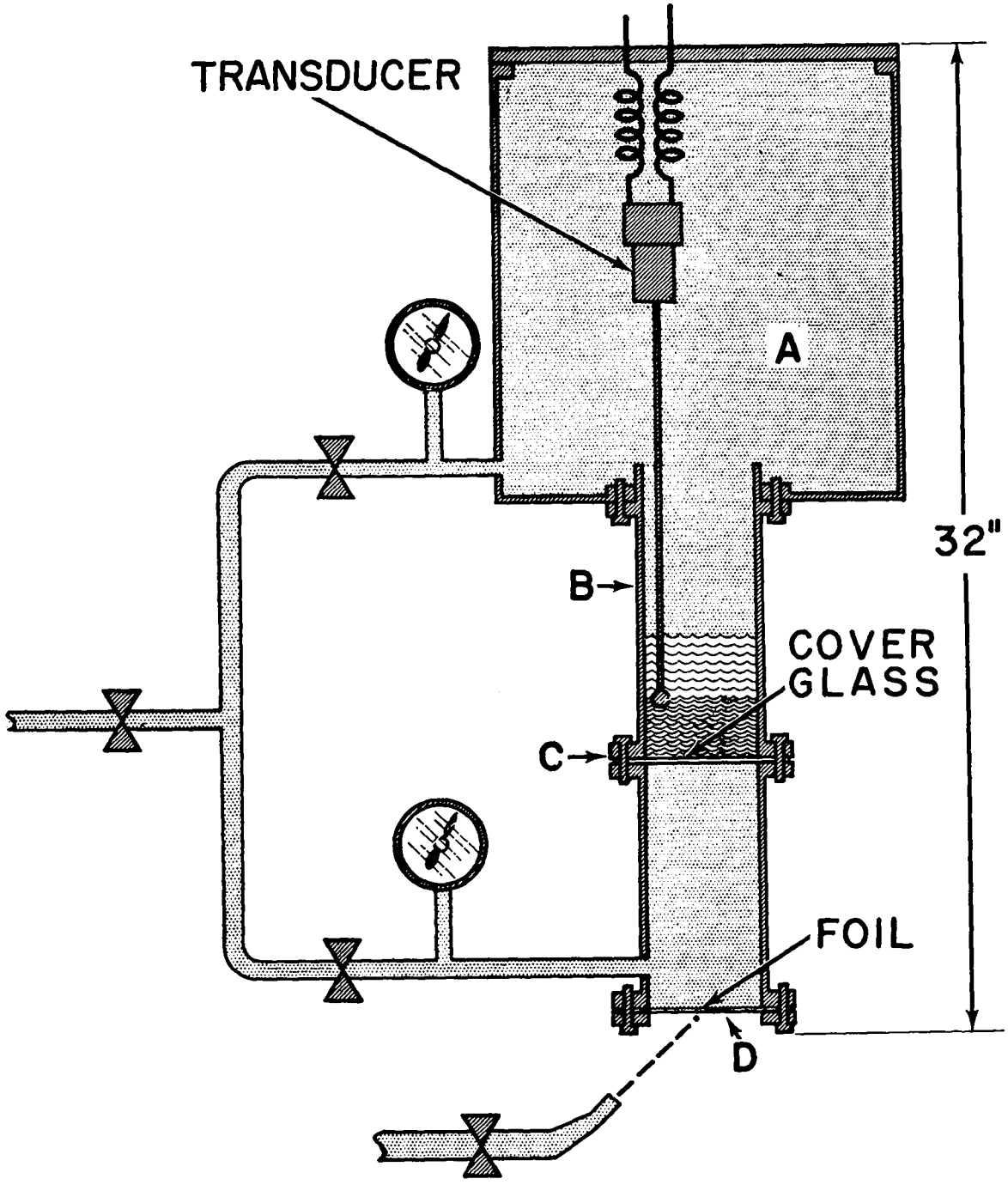

Fig. 4.1. Lewis machine.

Film No.	Wave Length cm	Density ρ_1	Density ρ_2	Density $(\rho_2-\rho_1)/(\rho_2+\rho_1)$	Surface Tension dyne/cm	Viscosity μ_1 10^{-3} dyne sec/cm^2	Viscosity μ_2 10^{-3} dyne sec/cm^2	Acceleration in g's	Theor. α	[+] Limiting $\ddot{\eta}$ in g's	η_x^o cm
		cgs	cgs	cgs							
89	1.0	.684	1.	.188	39.	4.1	10.	24.9	146	.33	.8
88	0.7	.684	1.	.188	39.	4.1	10.	27.8	161	1.6	2.
D-8	1.0	.827	1.	.095	8.5	89.	10.	62.3	178	2.8	2.
E-1	0.4	.827	1.	.095	8.5	89.	10.	42.7	193	--	.2
E-6	1.0	.684	1.	.188	1.	4.1	--	42.6	211	7.5	1.
D-5	0.7	.813	1.	.103	5.	40.	10.	58.5	215	.7	.4
G-4	0.7	.684	1.	.188	39.	4.1	10.	55.1	233	45.	5.
D-1	1.0	.684	1.	.188	39.	4.1	10.	67.4	267	1.2	2.
D-2	0.7	.684	1.	.188	39.	4.1	10.	60.1	281	4.8	3.
G-5	1.0	.684	1.	.188	39.	4.1	10.	132.	~350	27.	2.
E-5	1.2	~.002	.684	.995	20.	.4	4.1	58.7	374	58.	9.

[+] Acceleration after initial growth obeys parabolic law

[o] Amplitude at which mushrooming begins

Fig. 4.2A. Properties of interfaces and results of measurements under uniform acceleration.

Film No.	Interface	Wave Length in cm	Density Factor $(\rho_2-\rho_1)/(\rho_2+\rho_1)$	Acceleration in g's	Exp.	α Theor.	% Difference
89	Water-n Heptane	1.0	.188	24.9	^{o} 195	146	+34
88	Water-n Heptane	0.7	.188	27.8	$^{+}$ 232 113	161	+44 -30
D-8	Water-Octyl Alc.	1.0	.095	62.3	110	178	-38
E-1	Water-Octyl Alc.	0.4	.095	42.7	^{o} 106	193	-45
E-6	Aerosol-n Heptane	1.0	.188	42.6	124	211	-41
D-5	Water-Iso Amyl Alc.	0.7	.103	58.5	^{o} 82	215	-62
G-4	Water-n Heptane	0.7	.188	55.1	143	233	-39
D-1	Water-n Heptane	1.0	.188	67.4	$^{+}$ 245 185	267	- 8 -31
D-2	Water-n Heptane	0.7	.188	60.1	194	281	-31
G-5	Water-n Heptane	1.0	.188	132.	209	~348	-40
E-5	n Heptane-Air	1.2	1.0	58.7	270	374	-28

^{o} Data poor : $^{+}$ Values for different waves, lower figure thought to be more reliable.

Fig. 4.2B. Properties of interfaces and results of measurements under uniform acceleration.

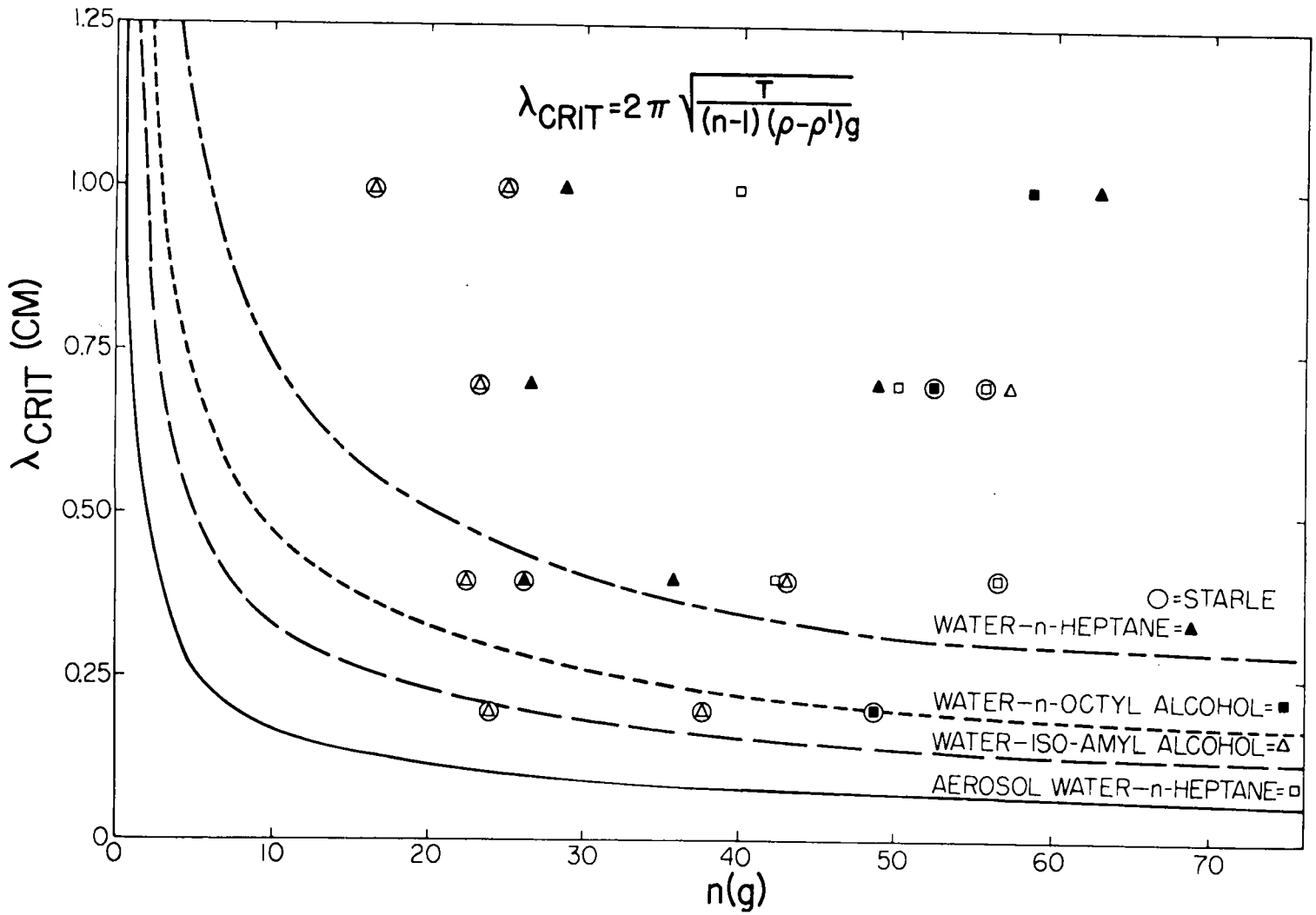

Fig. 4.3. Critical wavelength vs acceleration.

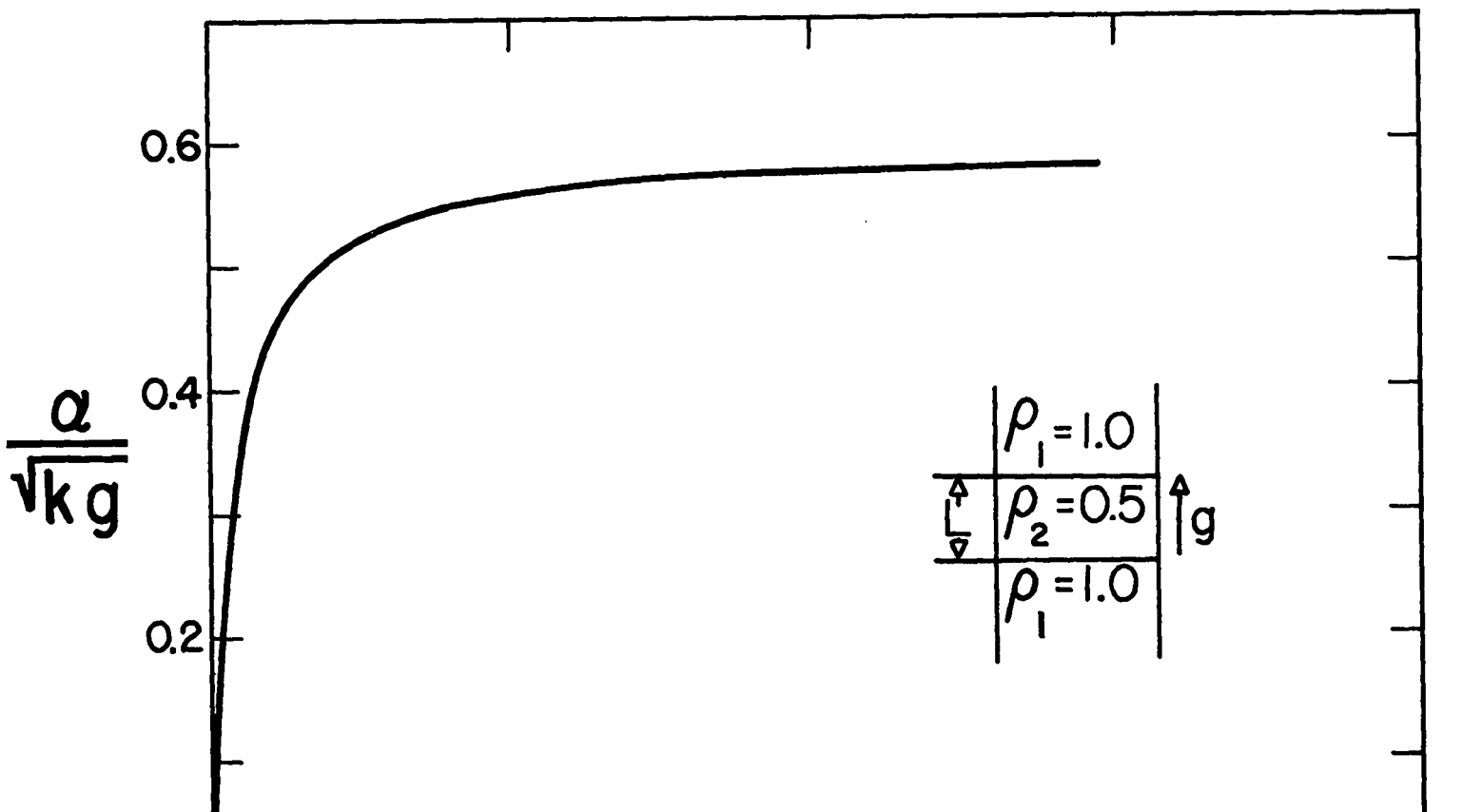

Fig. 4.4. The variation of α caused by density changes near the interface (results of calculations by D. S. Carter). The nature of the density variations are shown in the sketches, where g indicates the direction of the acceleration and L the extent of the density variation.

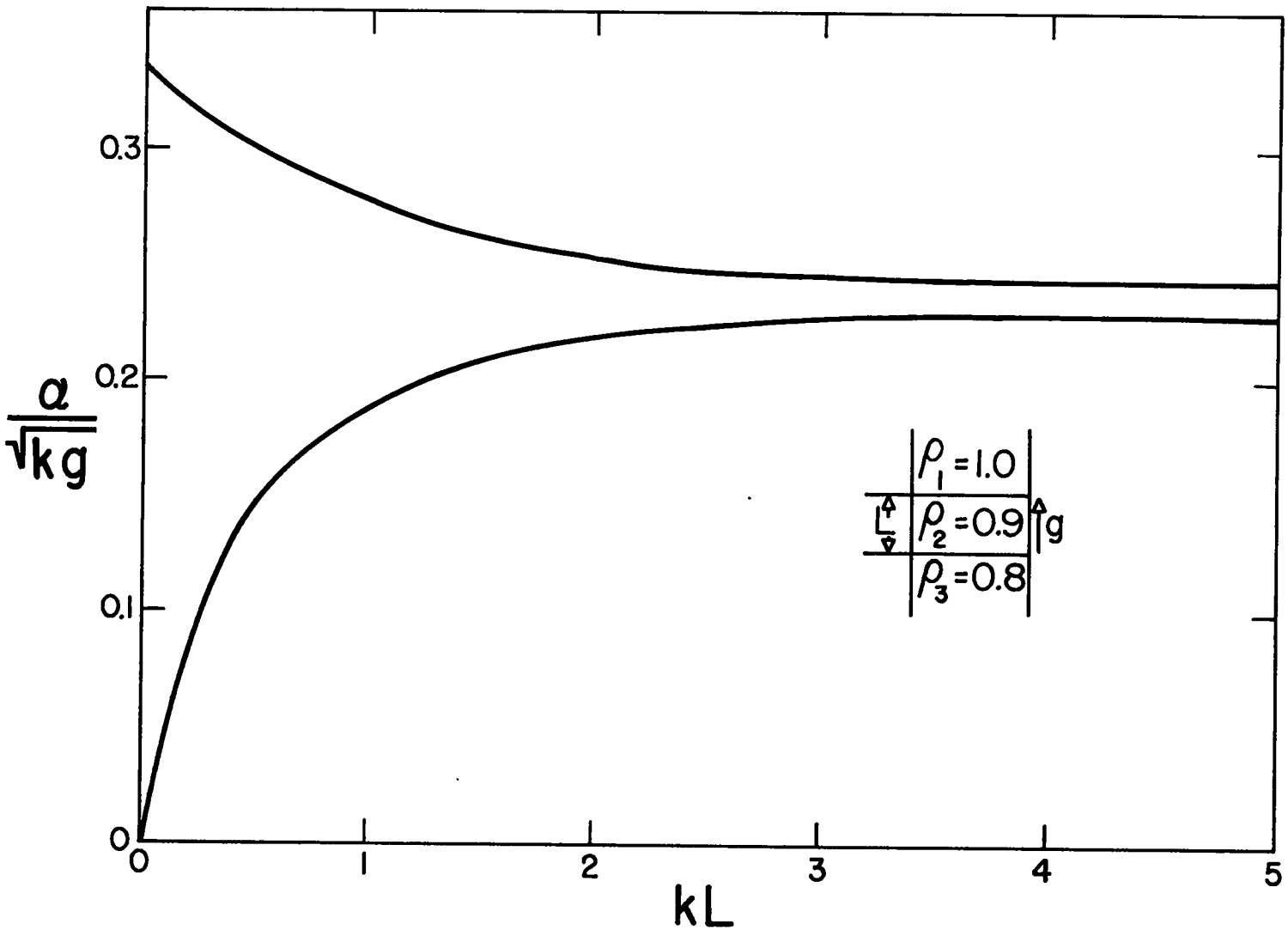

Fig. 4.5. The variation of α caused by density changes near the interface (results of calculations by D. S. Carter). The nature of the density variations are shown in the sketches, where g indicates the direction of the acceleration and L the extent of the density variation.

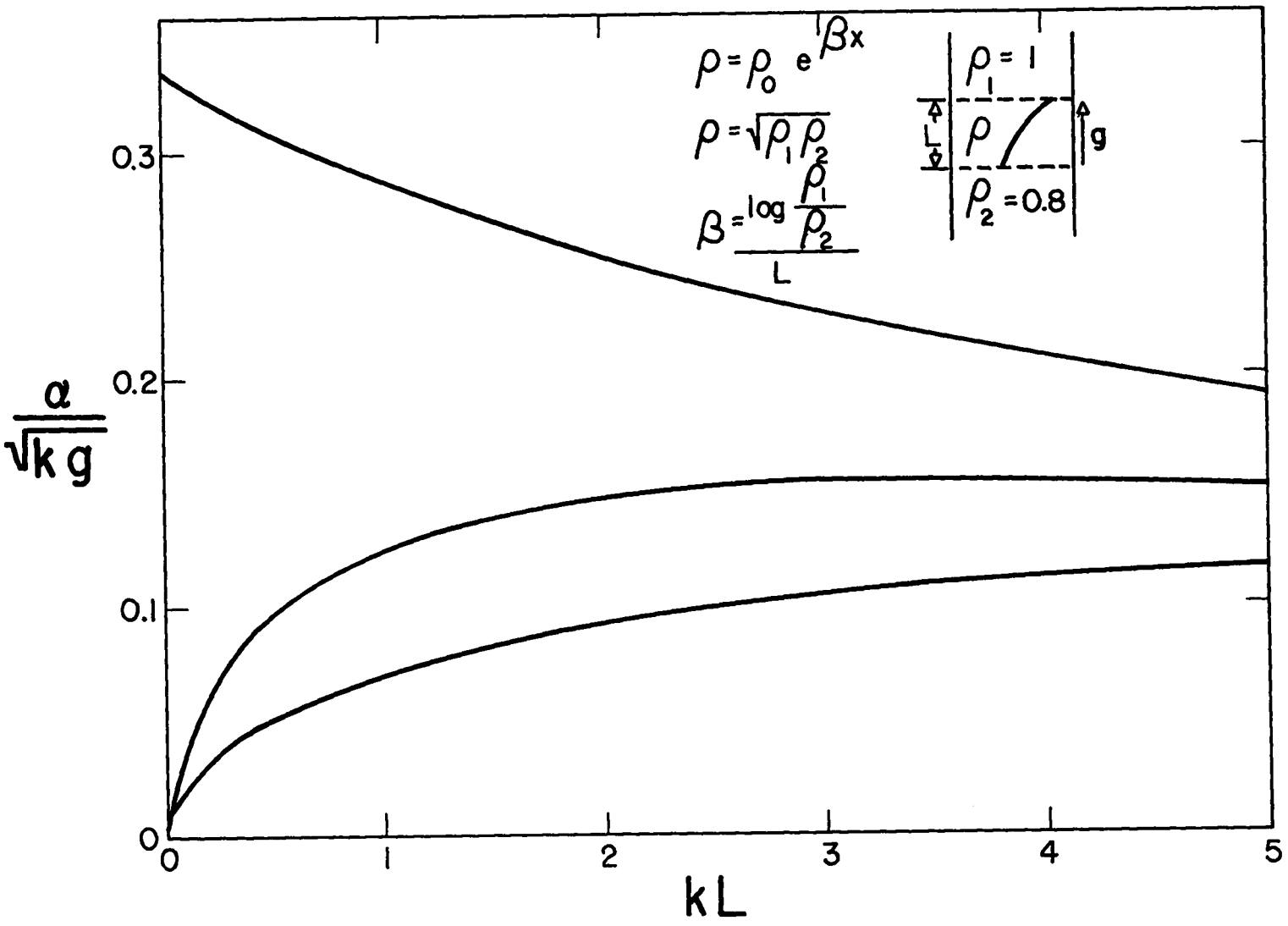

Fig. 4.6. The variation of α caused by density changes near the interface (results of calculations by D. S. Carter). The nature of the density variations are shown in the sketches, where g indicates the direction of the acceleration and L the extent of the density variation.

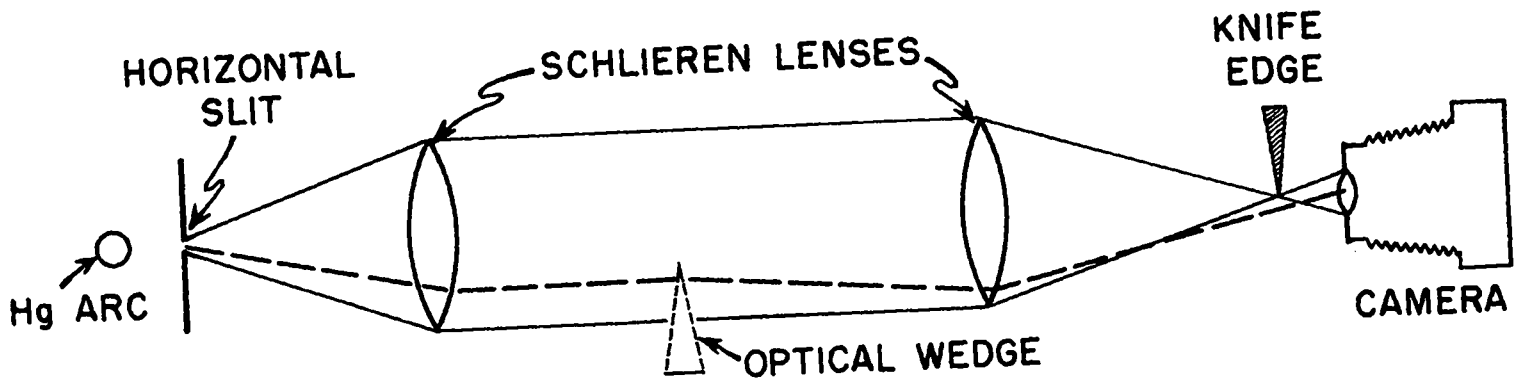

Fig. 4.7. Schlieren system.

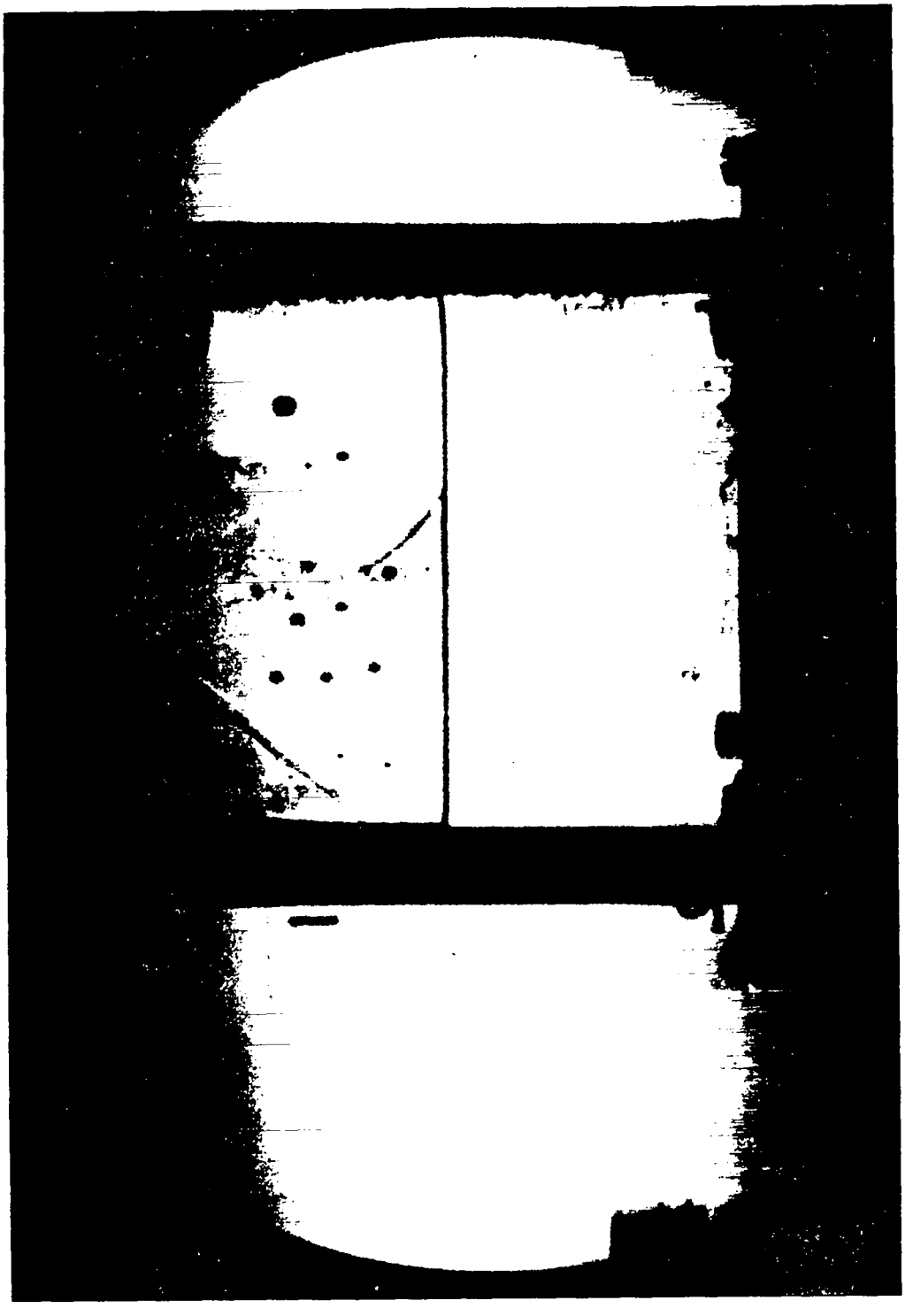

Fig. 4.8. Schlieren photograph showing water-isoamyl alcohol interface. Picture is taken before addition of the alcohol to the water.

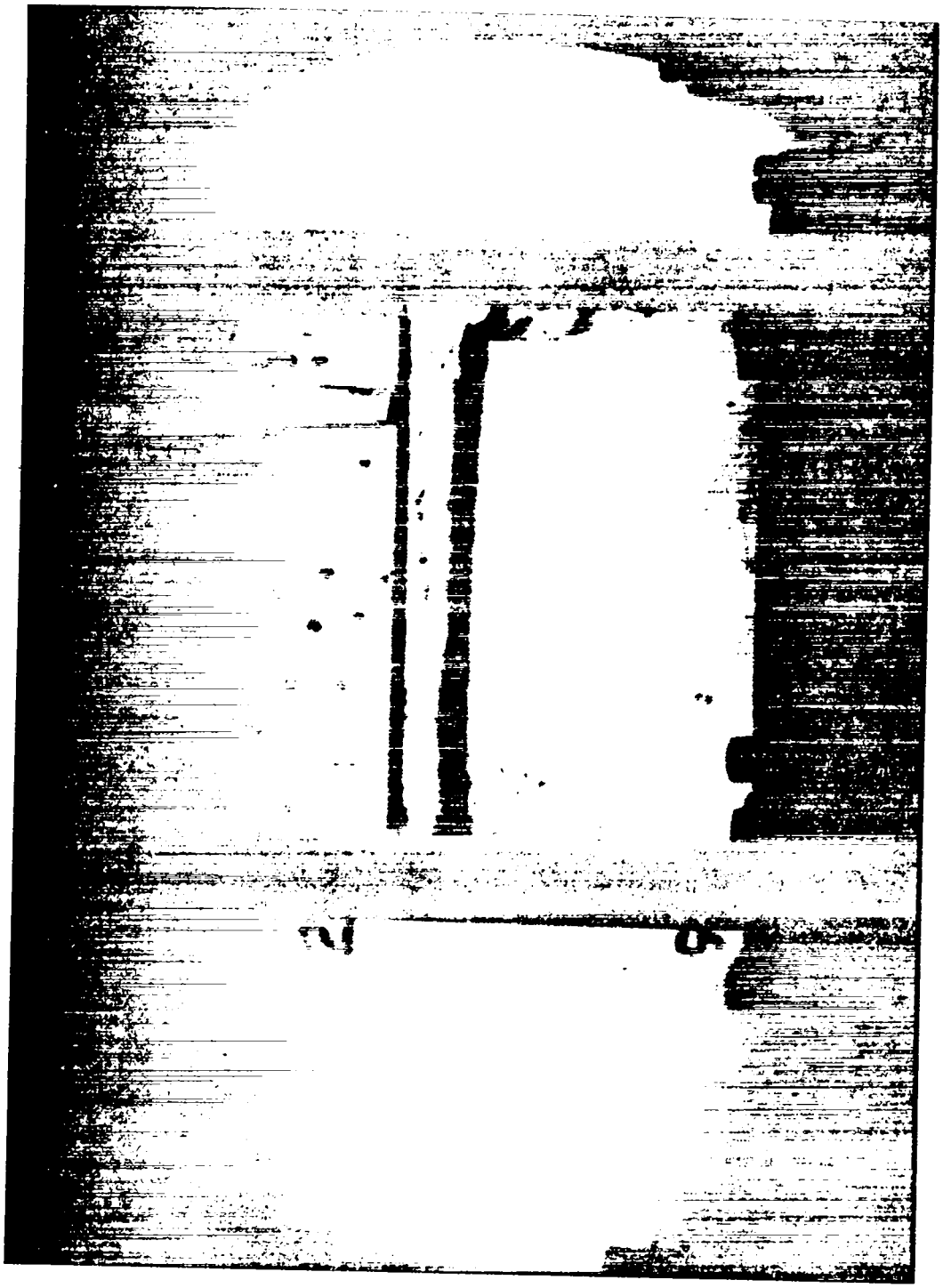

Fig. 4.9. Schlieren photograph showing water-isoamyl alcohol interface. Picture is taken just as alcohol is added to water.

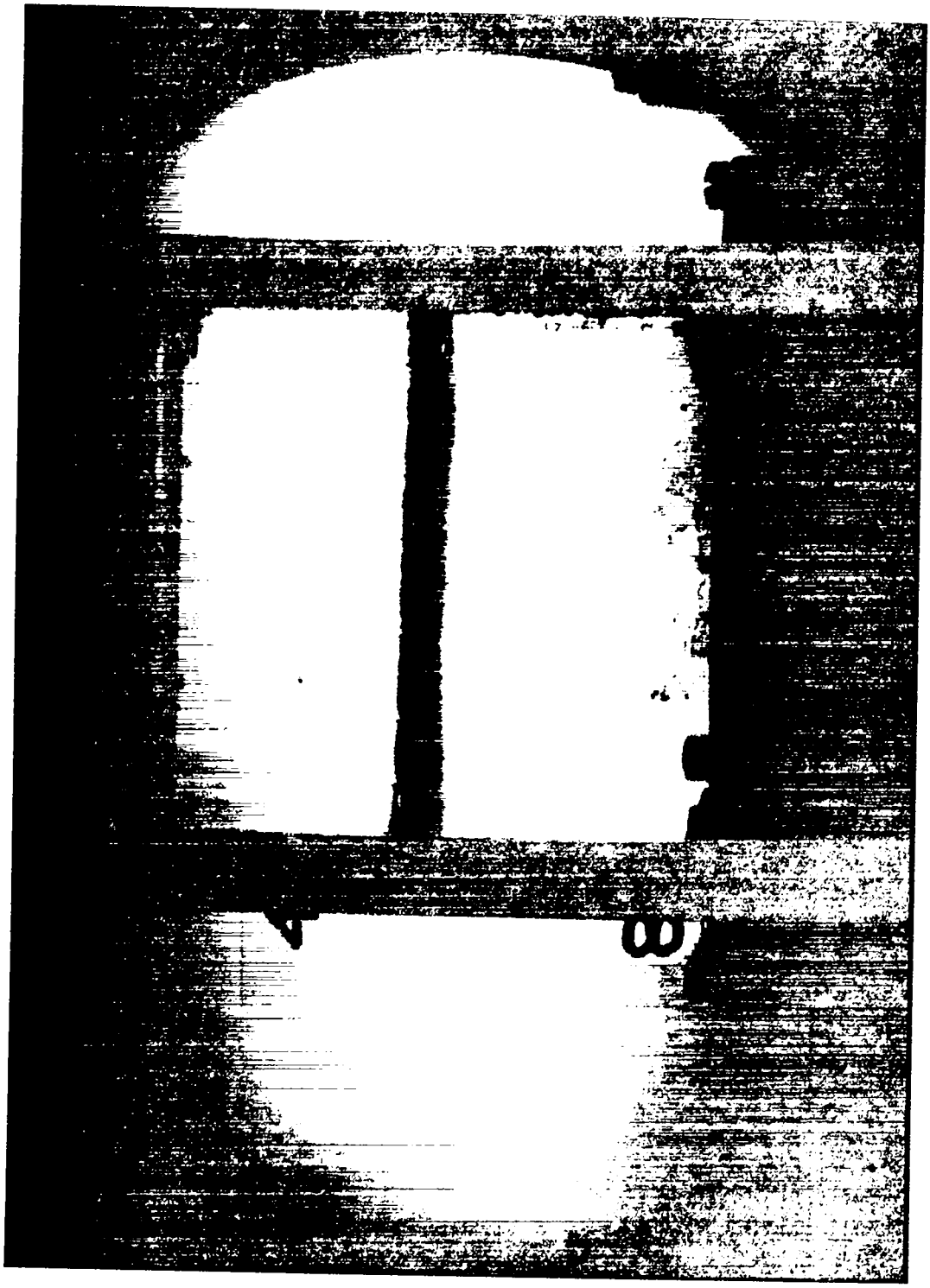

Fig. 4.10. Schlieren photograph showing water-isoamyl alcohol interface. Picture is taken 1 minute after addition of the alcohol to the water.

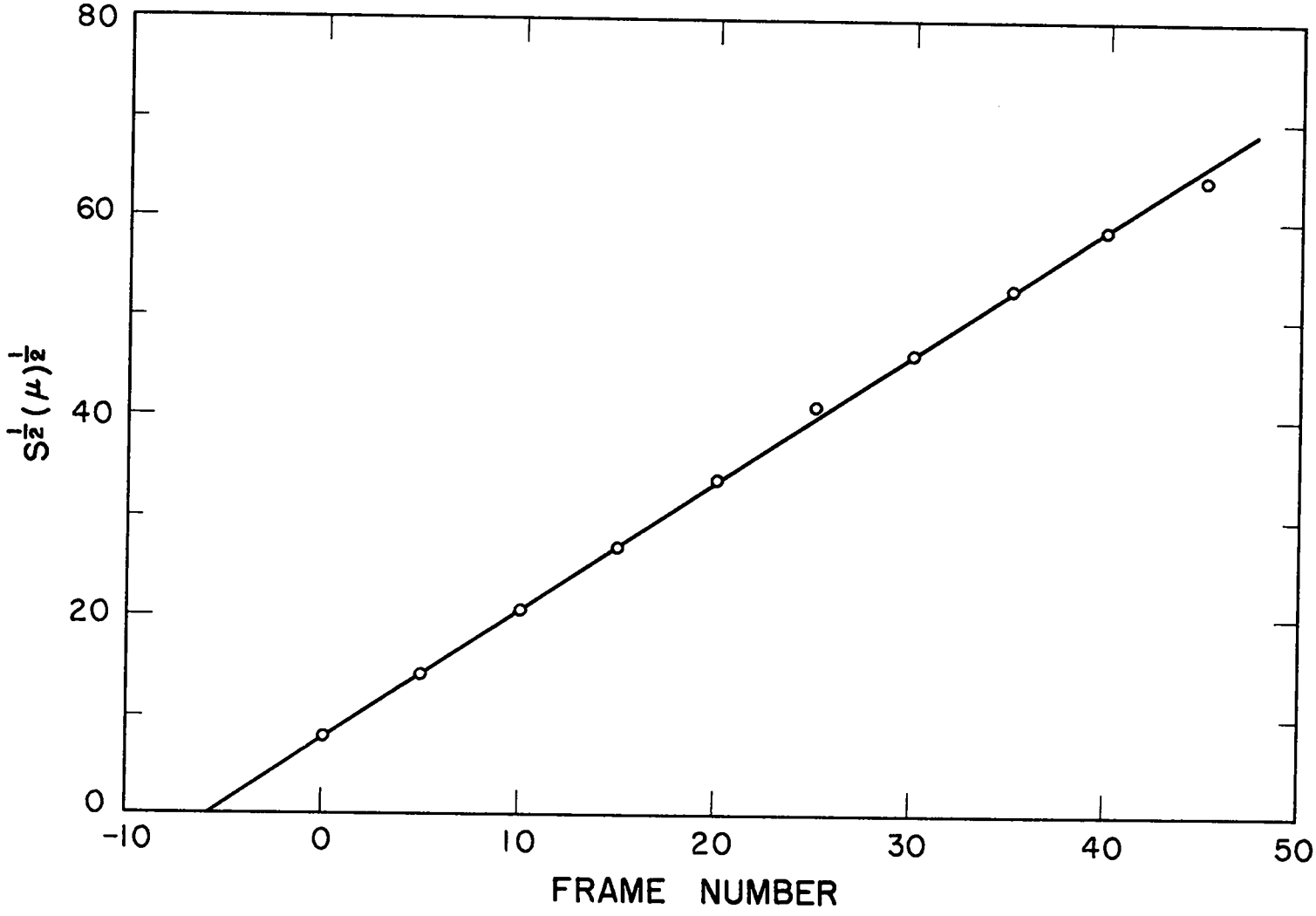

Fig. 4.11. Interface displacement vs frame number.

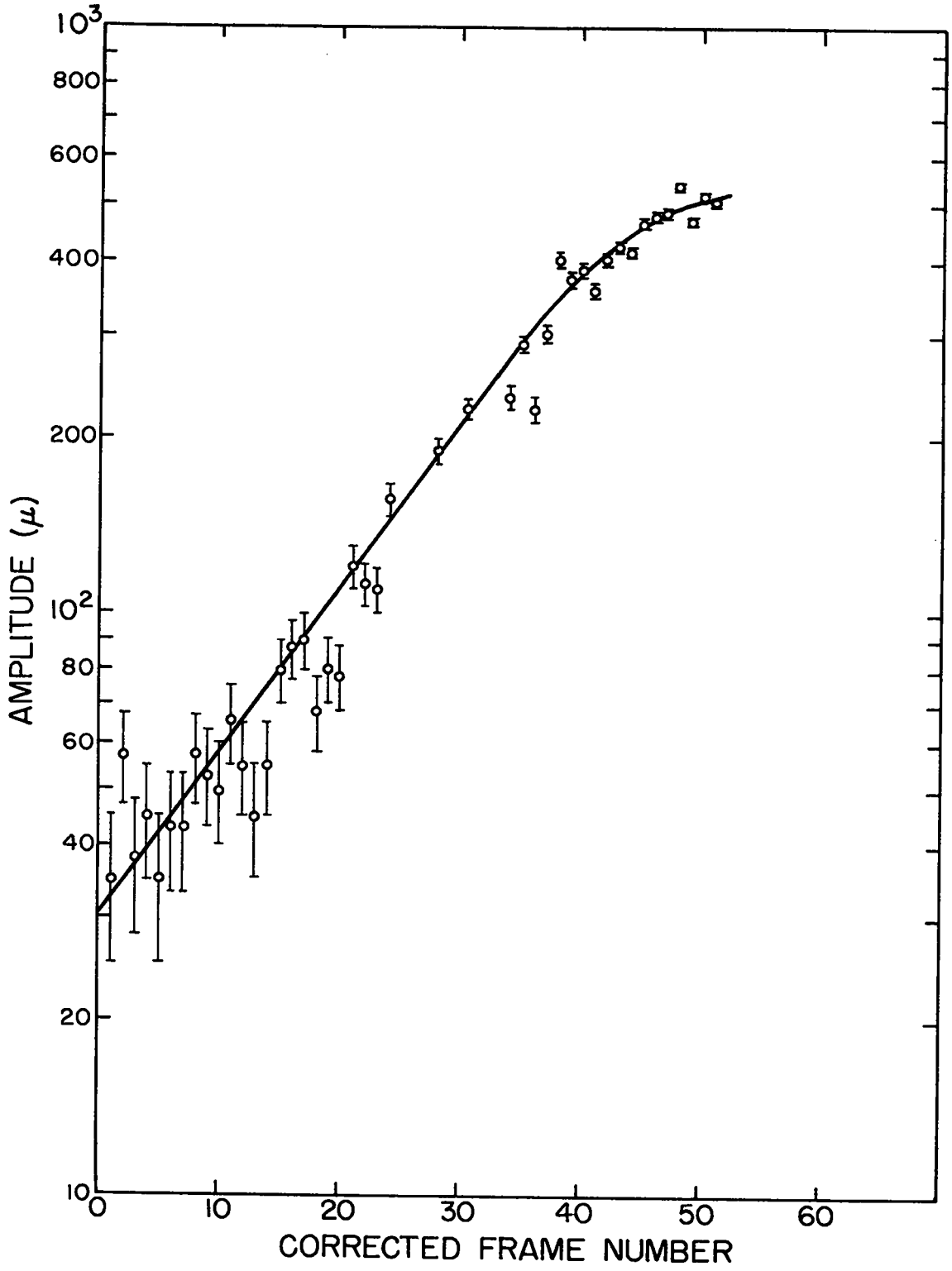

Fig. 4.12. Log amplitude vs frame number.

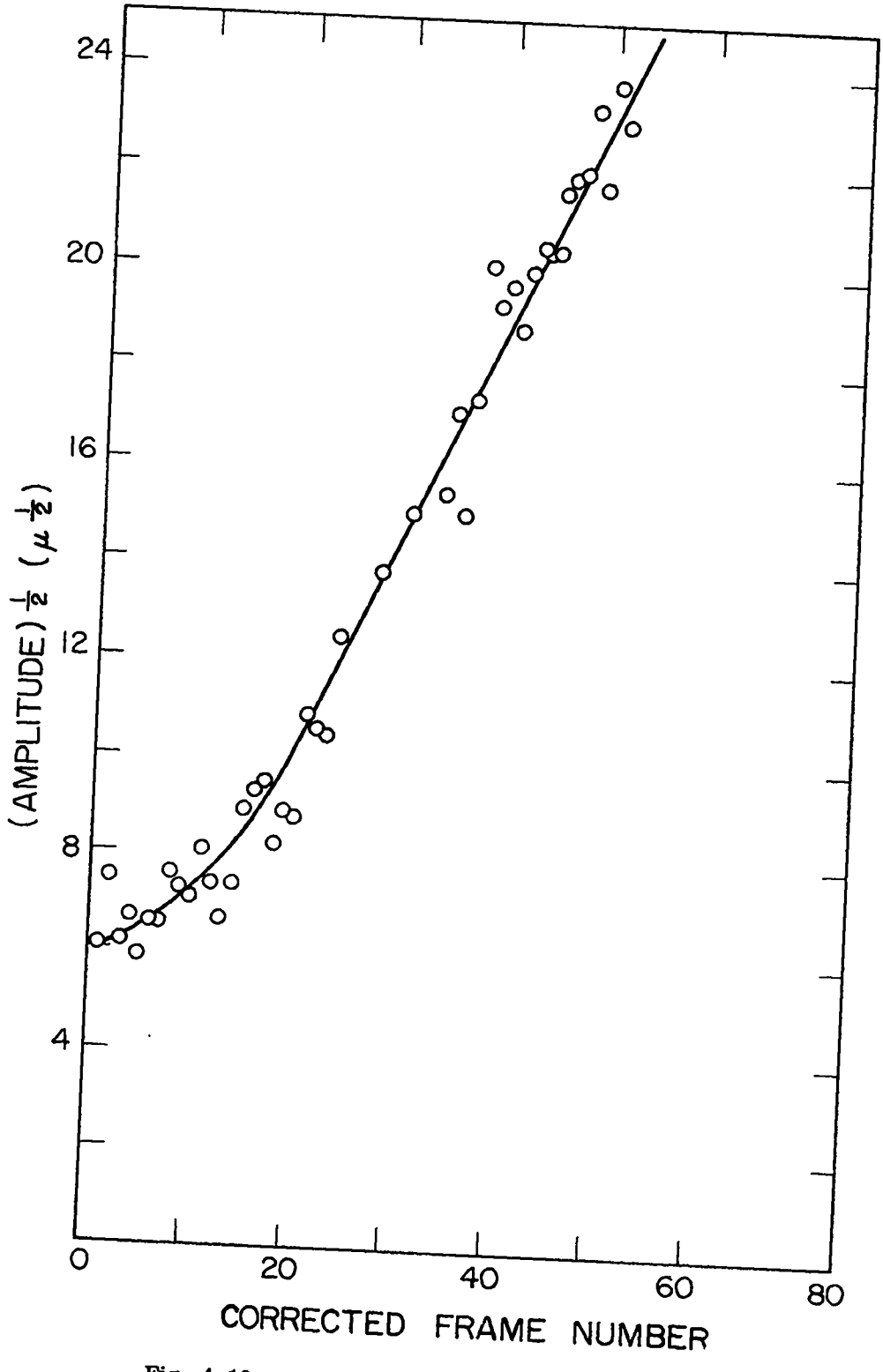

Fig. 4.13. Square root amplitude vs frame number.

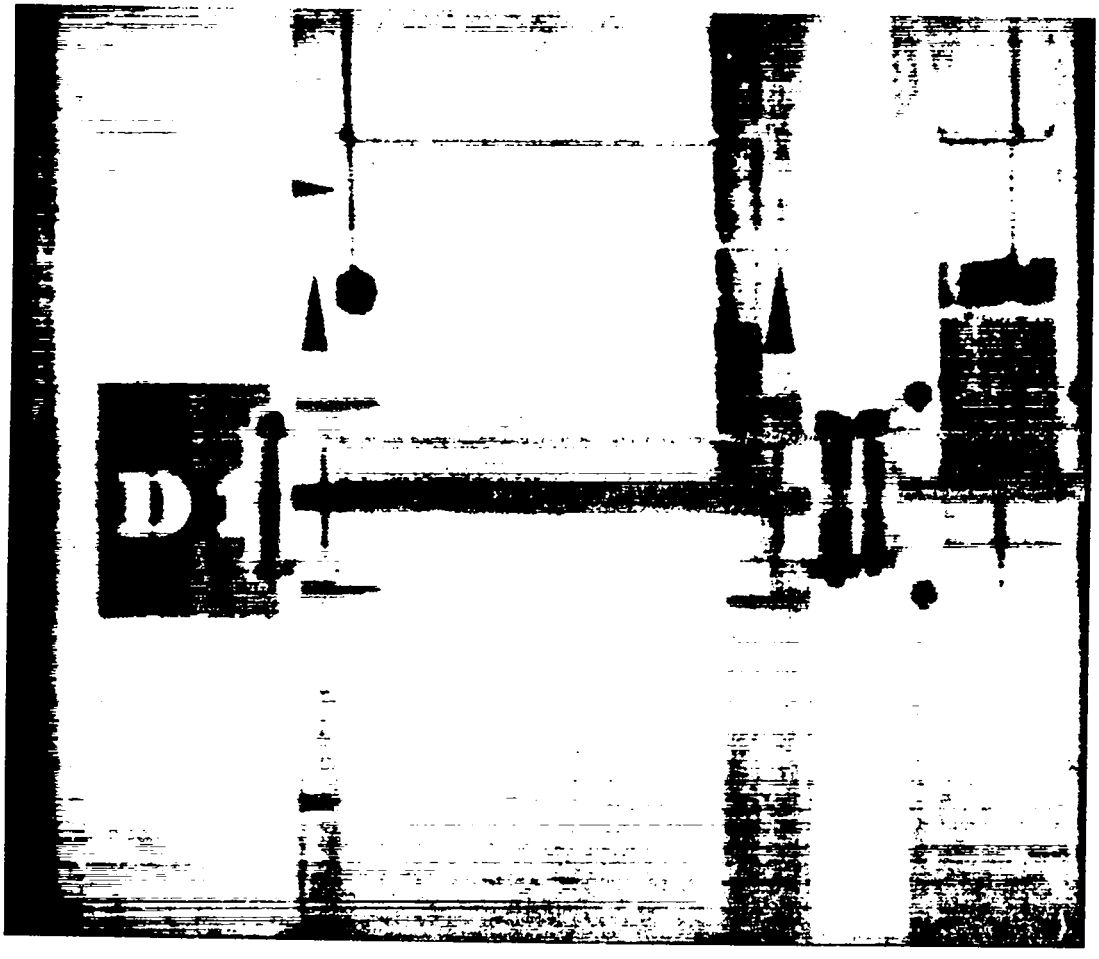

Fig. 4.14. The progression of Taylor instability on a water-n-heptane interface, under an acceleration of 67.4 g. The exposure is printed at frame number 0. One frame corresponds to a time interval of 0.355 msec (see also Fig. 4.2).

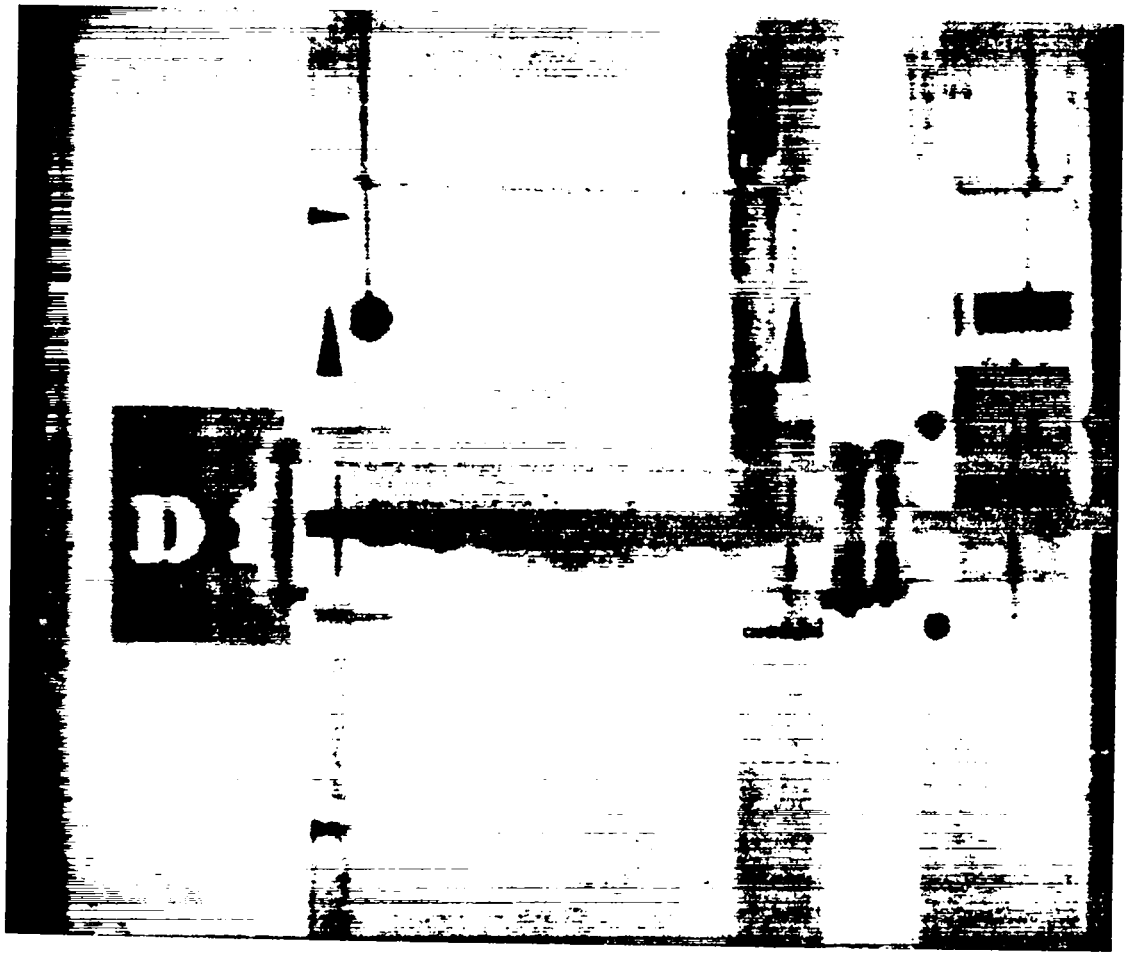

Fig. 4.15. The progression of Taylor instability on a water-n-heptane interface, under an acceleration of 67.4 g. The exposure is printed at frame number 5. One frame corresponds to a time interval of 0.355 msec (see also Fig. 4.2).

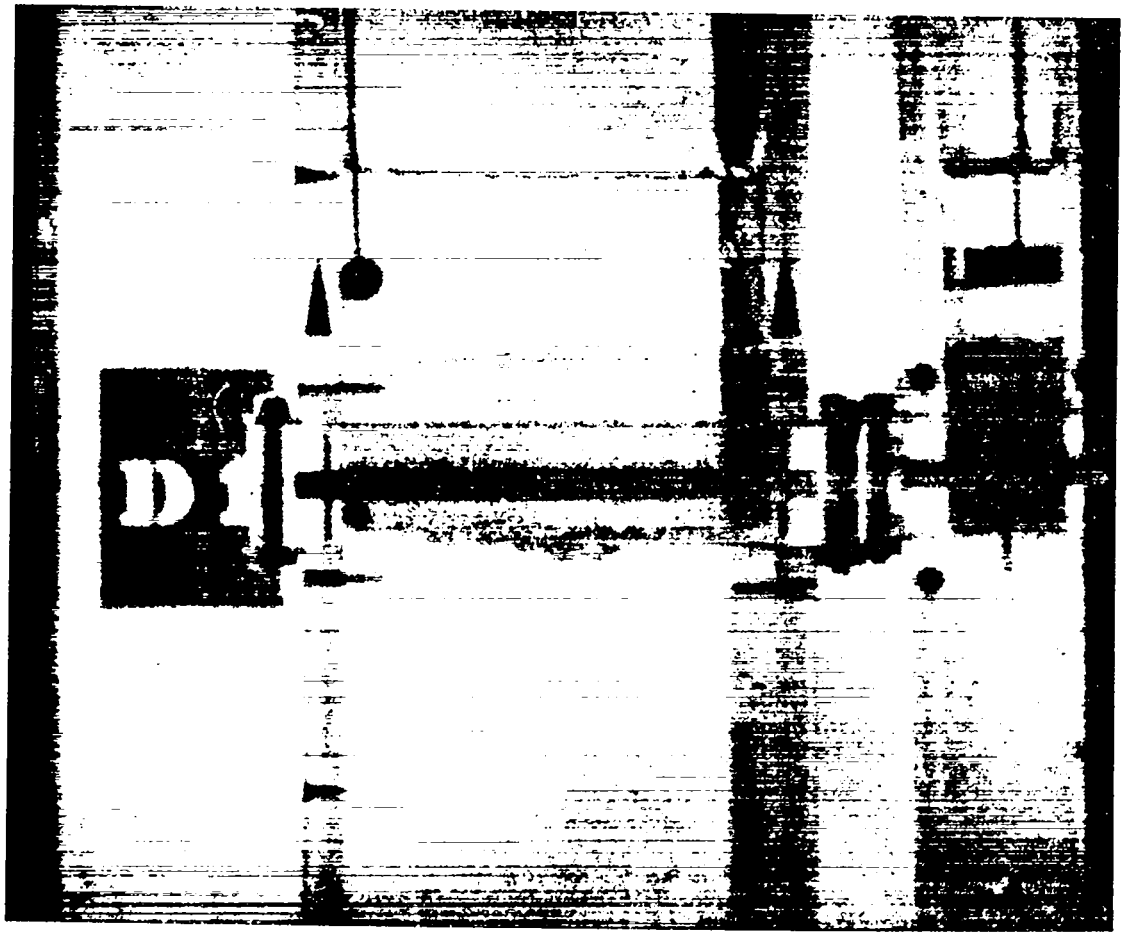

Fig. 4.16. The progression of Taylor instability on a water-n-heptane interface, under an acceleration of 67.4 g. The exposure is printed at frame number 10. One frame corresponds to a time interval of 0.355 msec (see also Fig. 4.2).

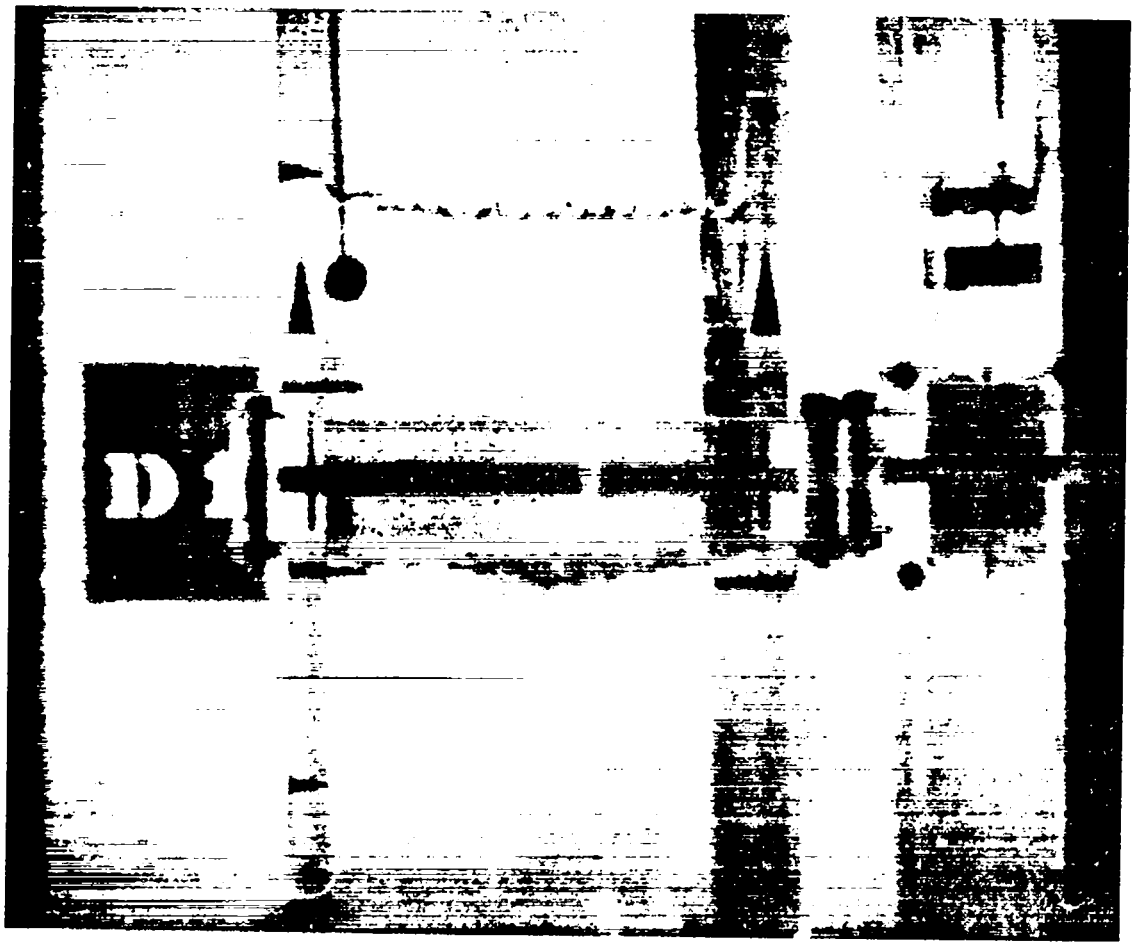

Fig. 4.17. The progression of Taylor instability on a water-n-heptane interface, under an acceleration of 67.4 g. The exposure is printed at frame number 15. One frame corresponds to a time interval of 0.355 msec (see also Fig. 4.2).

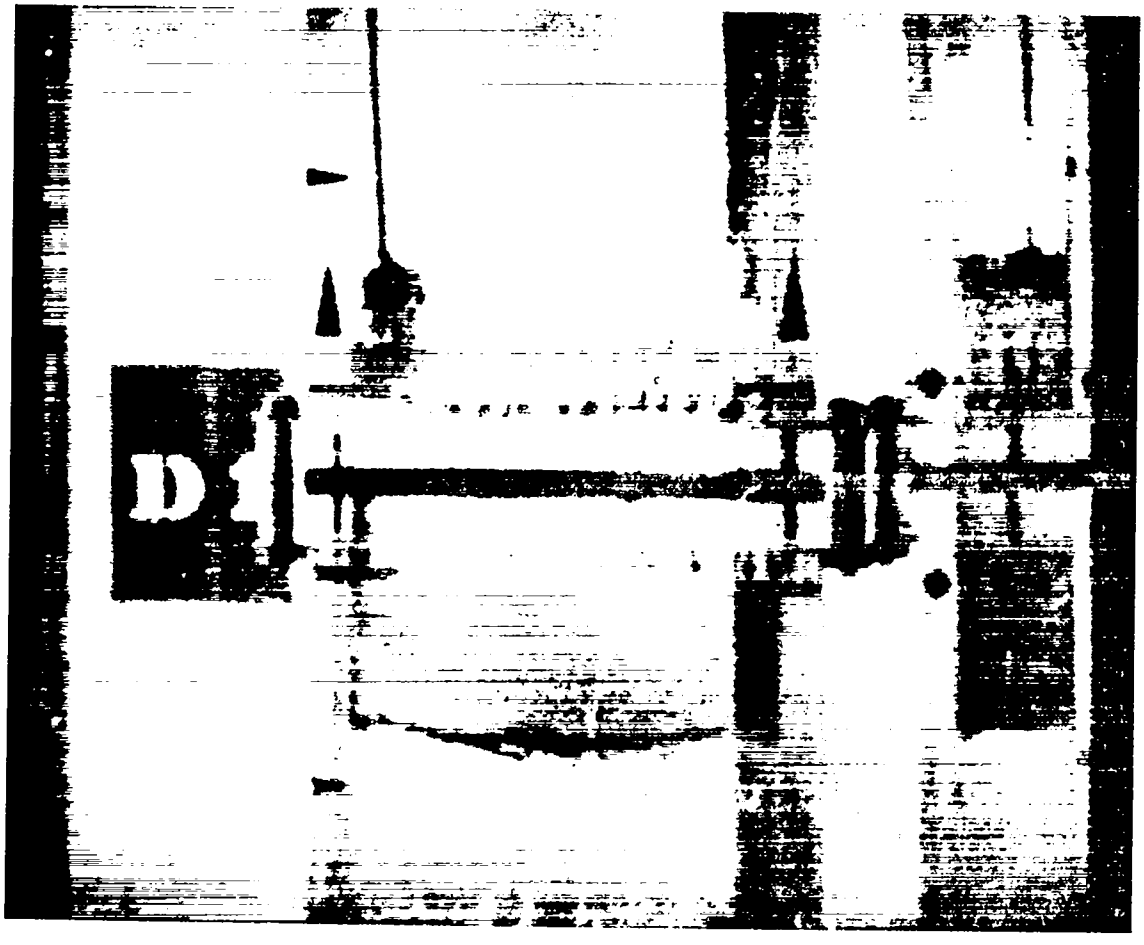

Fig. 4.18. The progression of Taylor instability on a water-n-heptane interface, under an acceleration of 67.4 g. The exposure is printed at frame number 30. One frame corresponds to a time interval of 0.355 msec (see also Fig. 4.2).

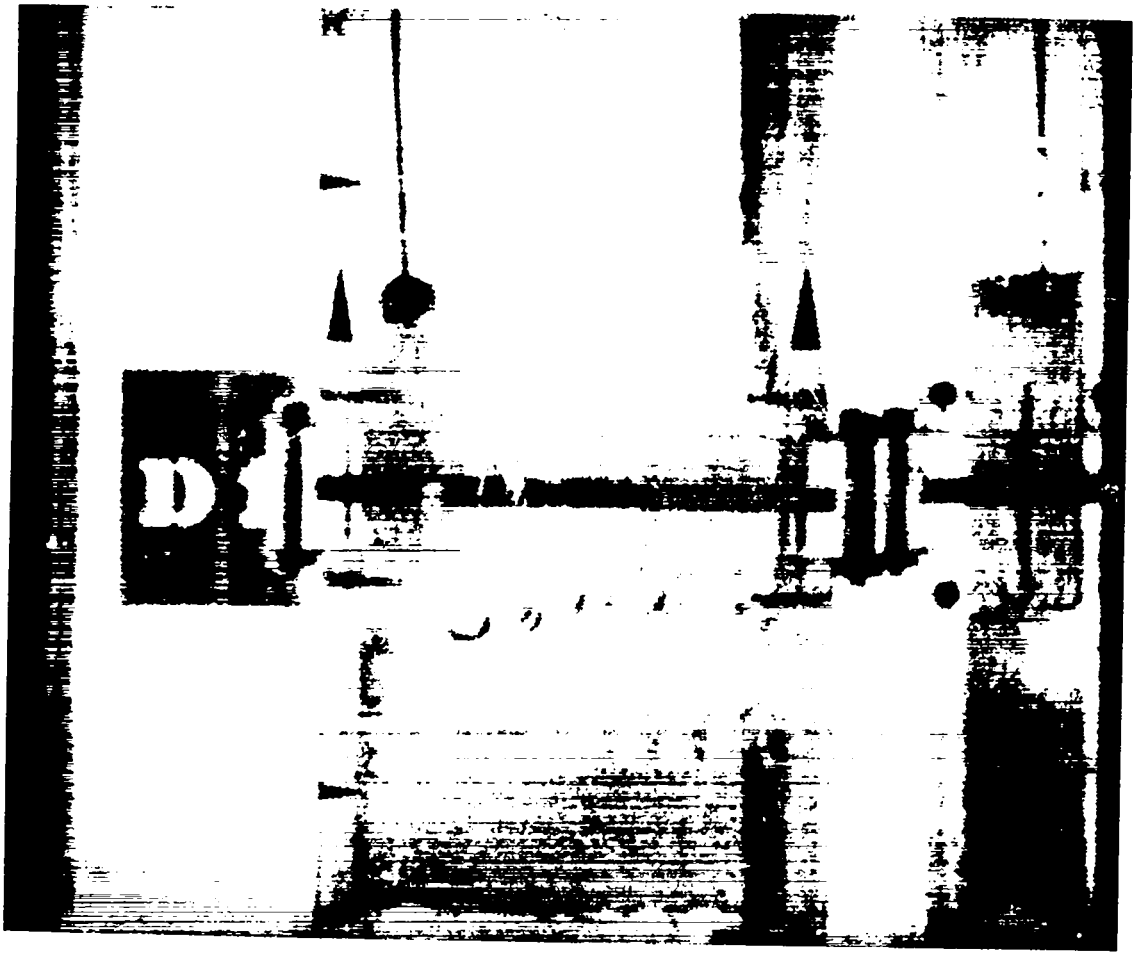

Fig. 4.19. The progression of Taylor instability on a water-n-heptane interface, under an acceleration of 67.4 g. The exposure is printed at frame number 40. One frame corresponds to a time interval of 0.355 msec (see also Fig. 4.2).

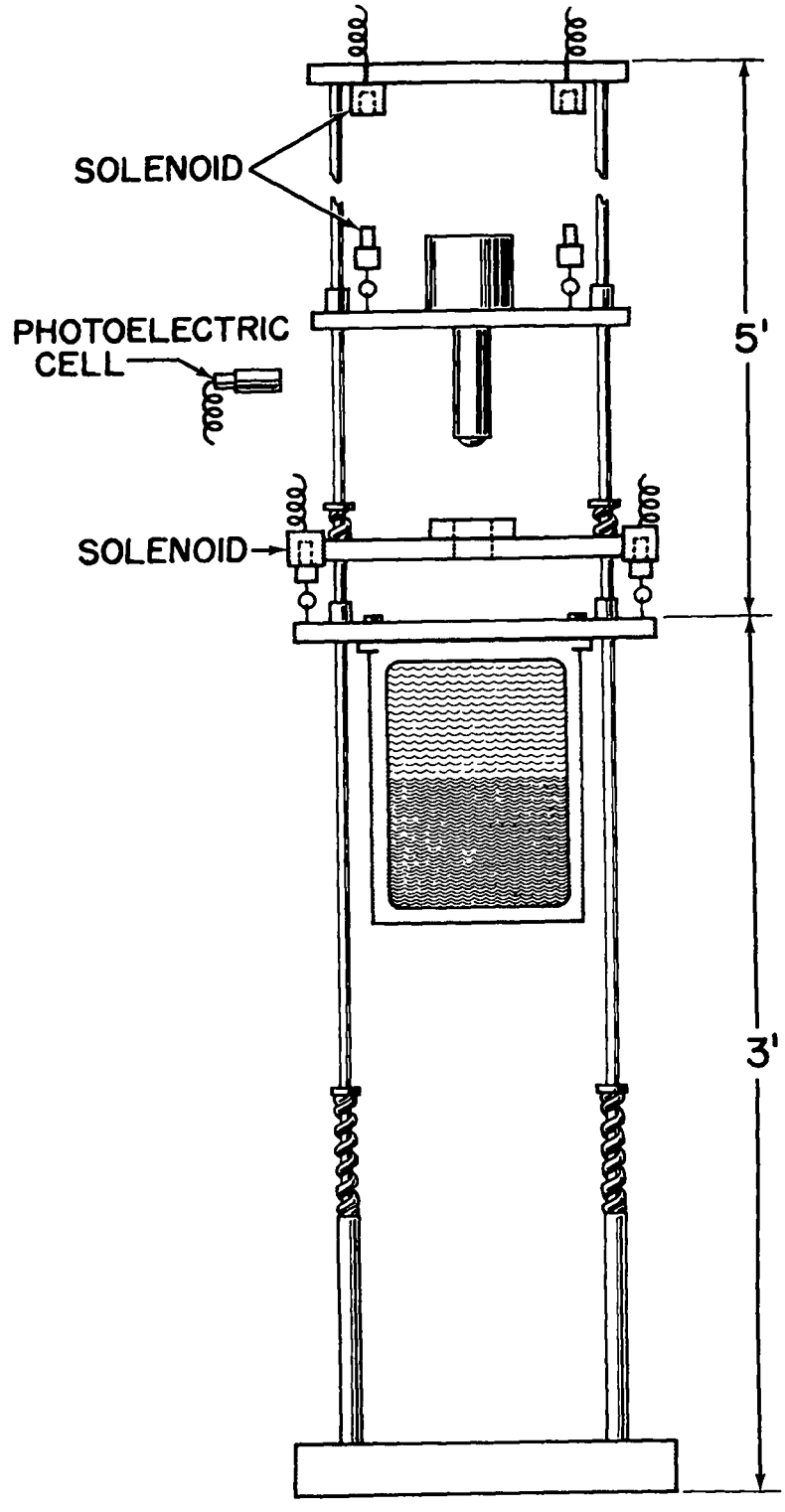

Fig. 5.1. Impulse apparatus.

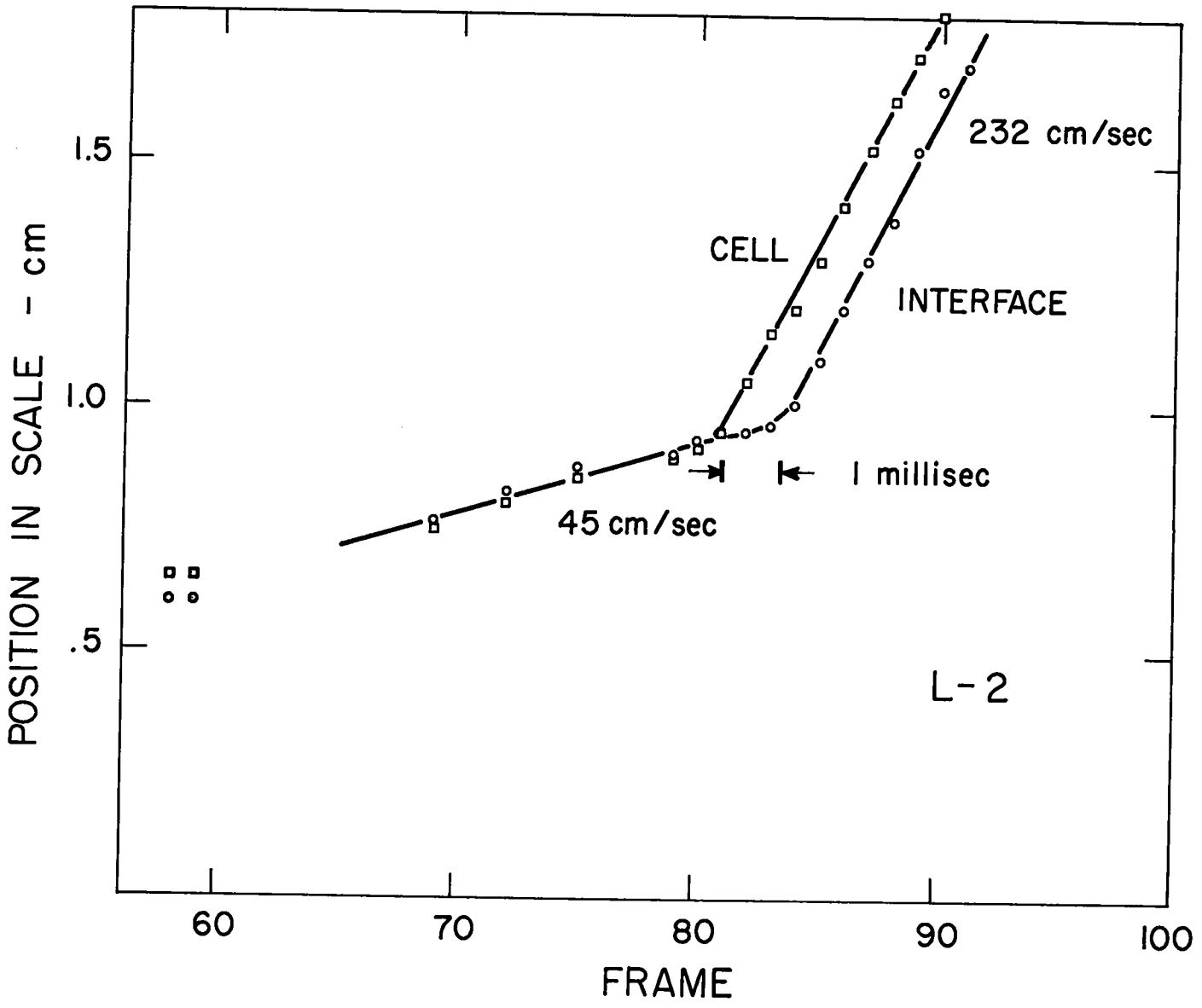

Fig. 5.2. Interface and cell positions vs frame number. 1 cm = 0.975 scale cm and 2.71 frames correspond to 1 millisecond.

Film	Liquids	Initial λ cm	Acceleration g	Expected Growth Initial Amp / Final Amp	Actual Growth Initial Amp cm / Final Amp cm	λ_{danger} cm	λ_{spikes} cm	Max Speed of Spike Growth* cm/sec
I-2	Aerosol-n Heptane	none	119	--	--	~.08 This would appear as fuzz	Fuzz	--
K-5	Water-n Heptane	2.2	240	1.06	.50/.46 = 1.08 .19/.16 = 1.18	.247	.2< λ <.25	150
K-6	Water-n Heptane	2.6	252	1.06	.28/.26 = 1.07 .17/.16 = 1.06	.243	.25	187
L-2	Water-n Heptane	none	190	--	--	.278	.28	316

* These values determined for growth after initial cavitation. In L-2 the camera was timed with the impulse to view earlier in the growth than in K-5 and K-6.

Fig. 5.3. Summary of impulse data.

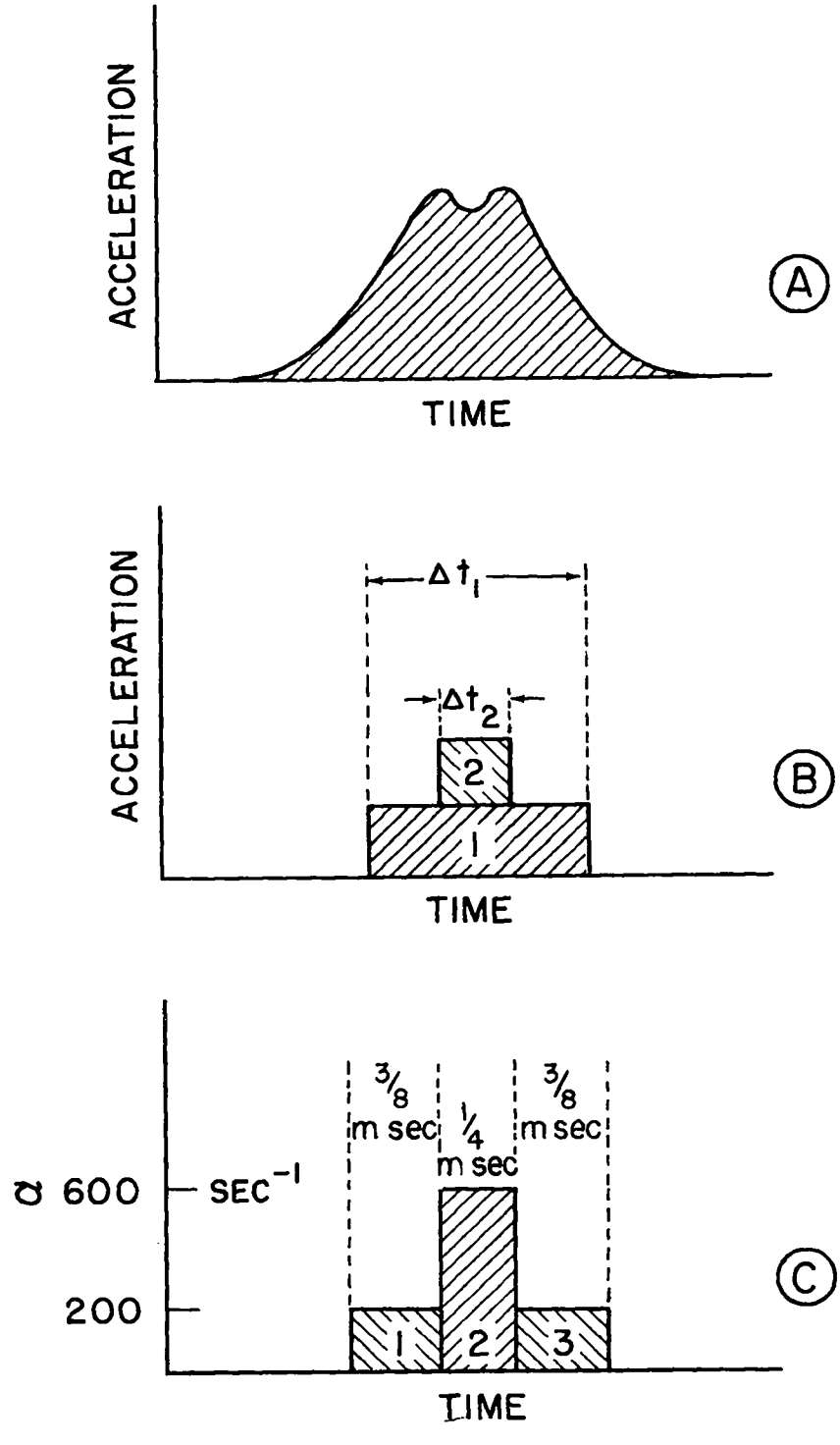

Fig. 5.4. Typical impulse forms.

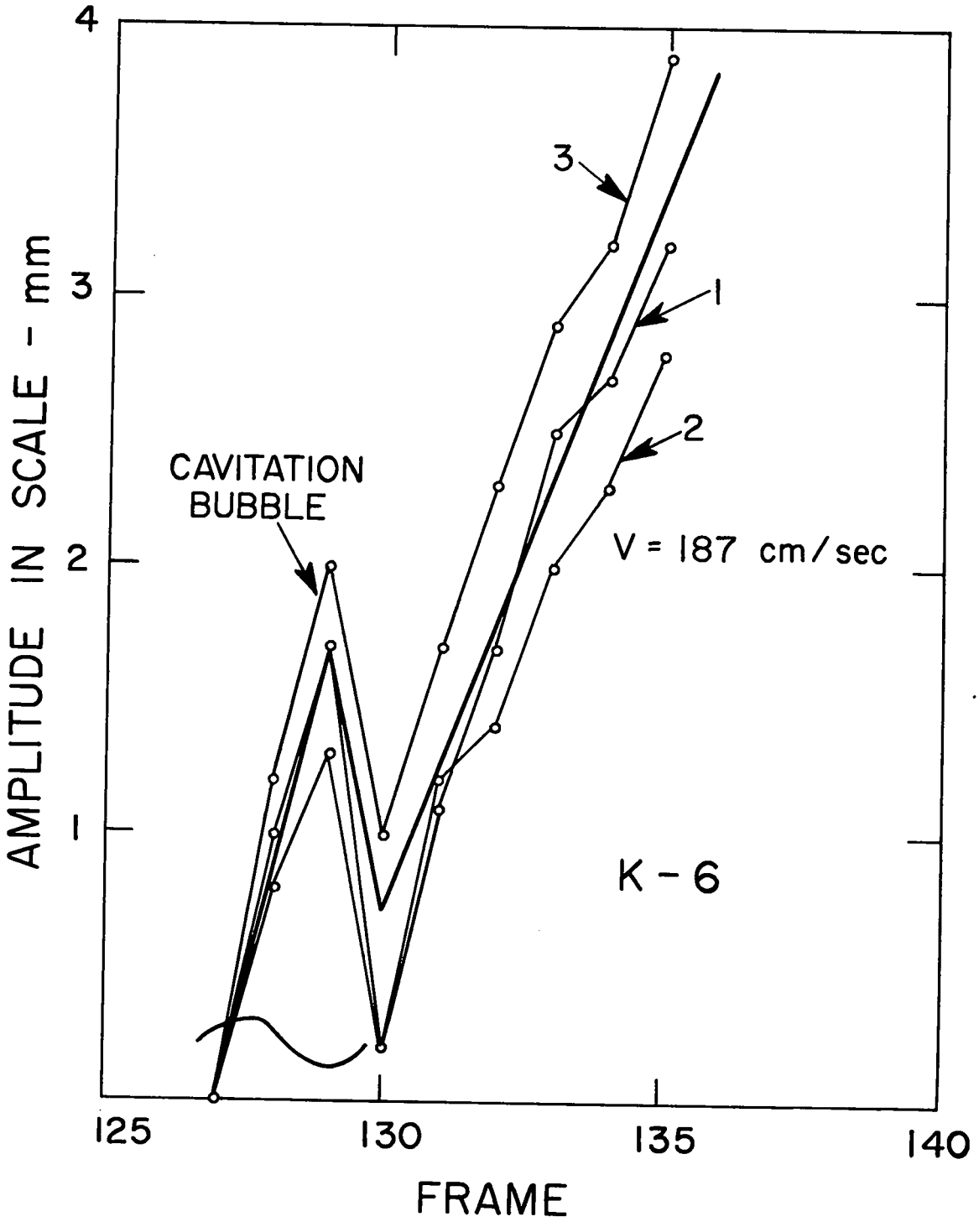

Fig. 5.5. Spike amplitude vs frame number. Growth of three separate spikes is shown.

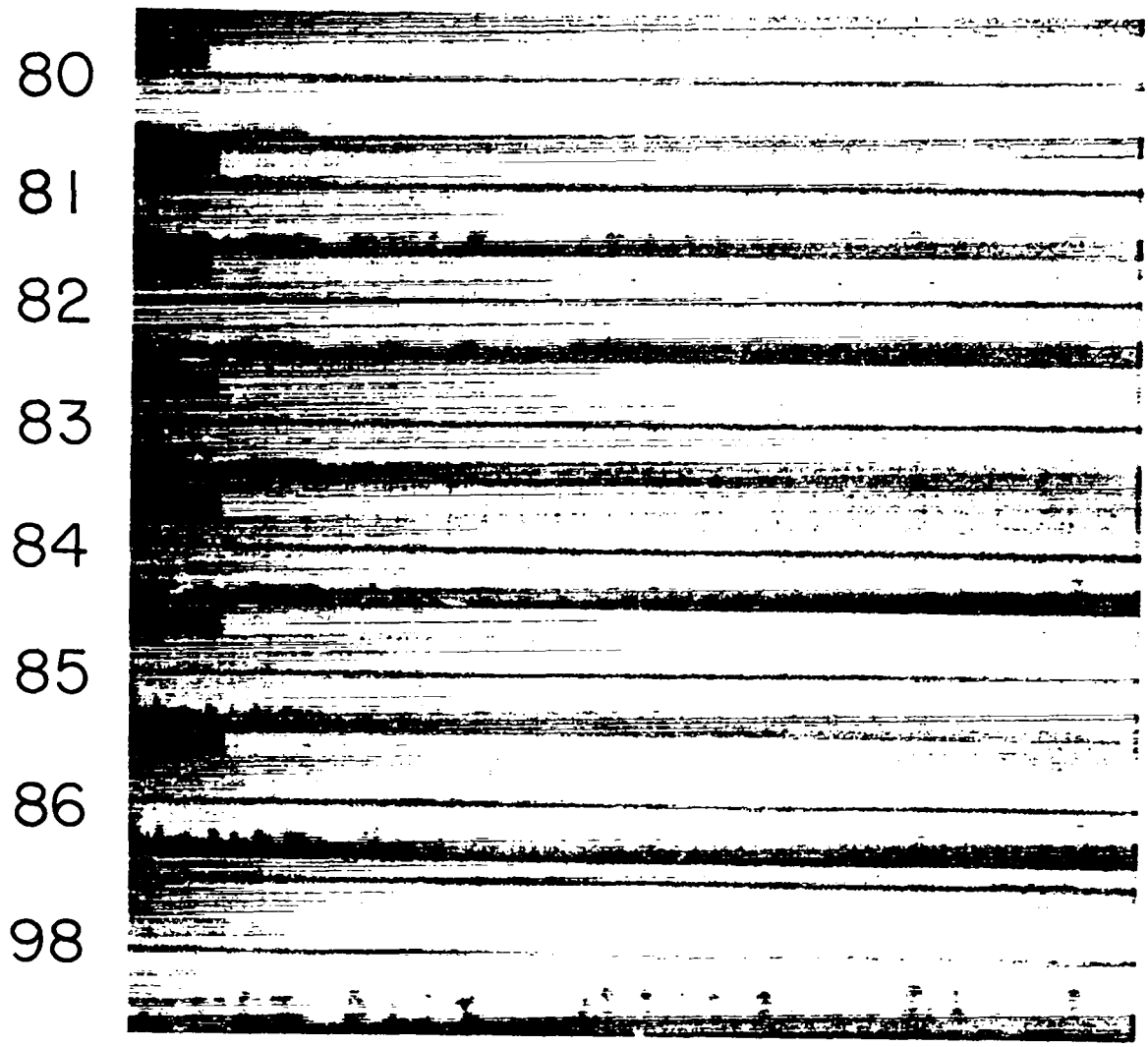

Fig. 5.6. Impulse L-2. A water-n-heptane interface under impulse. Number refer to film frame numbers (1 frame $\simeq 3 \cdot 10^{-4}$ sec). Grid in background is standard millimeter graph paper.

Fig. 5.7. Impulse K-6. A water-n-heptane interface photographed about 4.5 milliseconds after the impulse. Grid in background is standard millimeter graph paper.

APPENDIX A

In the experiments in uniform acceleration (Lewis apparatus) and impulsive acceleration, an initial wave was required on the interface being observed. Because of the wide range of frequencies and amplitudes desired, it seemed advisable to use electronic means to provide the driving force for the vibrating bob.

A block diagram of the circuit used is shown in Fig. A1. The difficulty of amplification of the very low frequencies desired was overcome by the use of a 2300 cps carrier, amplitude modulated at the desired low frequency. The carrier frequency, supplied by a Hewlett-Packard Model 200D oscillator, and the low frequency, supplied by a Hewlett-Packard Model 202A oscillator, were mixed in a nonlinear pentode circuit. The resulting signal was filtered so that it contained only the high frequency components. After amplification to a high power level, the signal was demodulated by a copper sulphide rectifier, filtered, and use to drive the bob.

The mixer circuit is shown in Fig. A2.

The bob itself was a solenoid, modified by the insertion of a spring into the solenoid core. This arrangement provided satisfactory action over the frequency range from zero to about 40 cps, a resonance being observed at 8 cps.

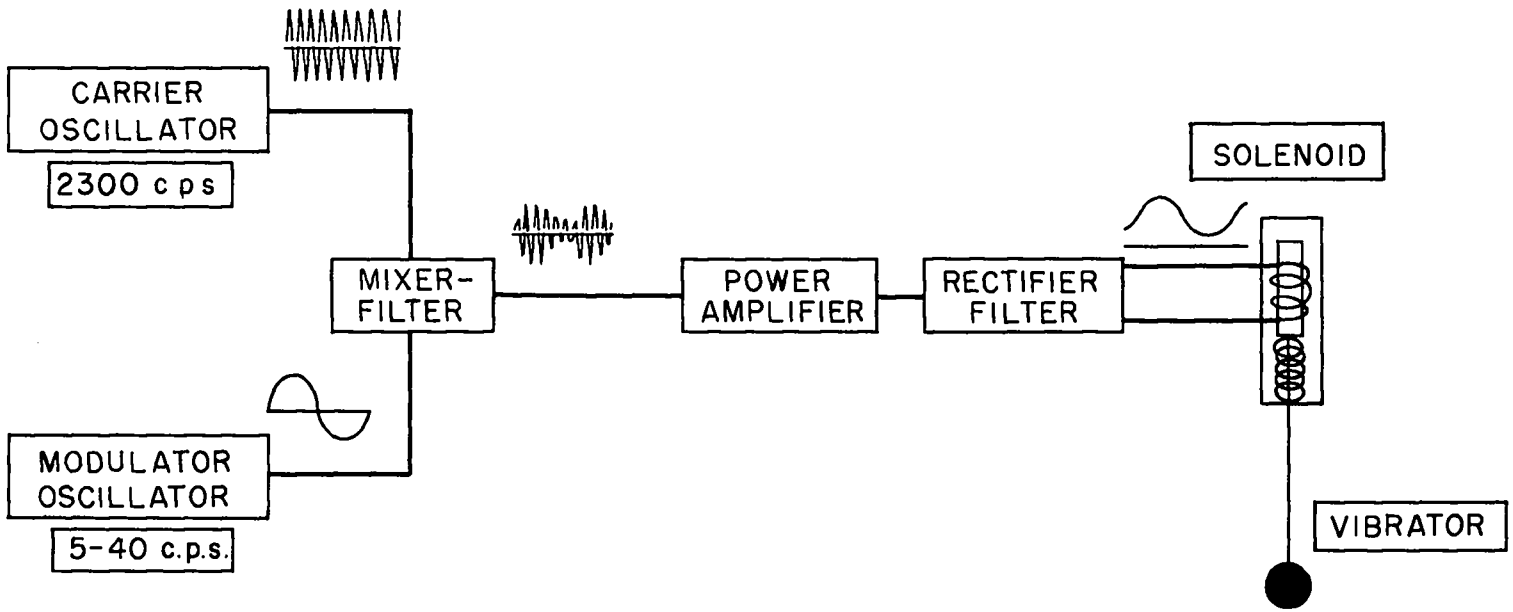

Fig. A1. Block diagram of transducer system.

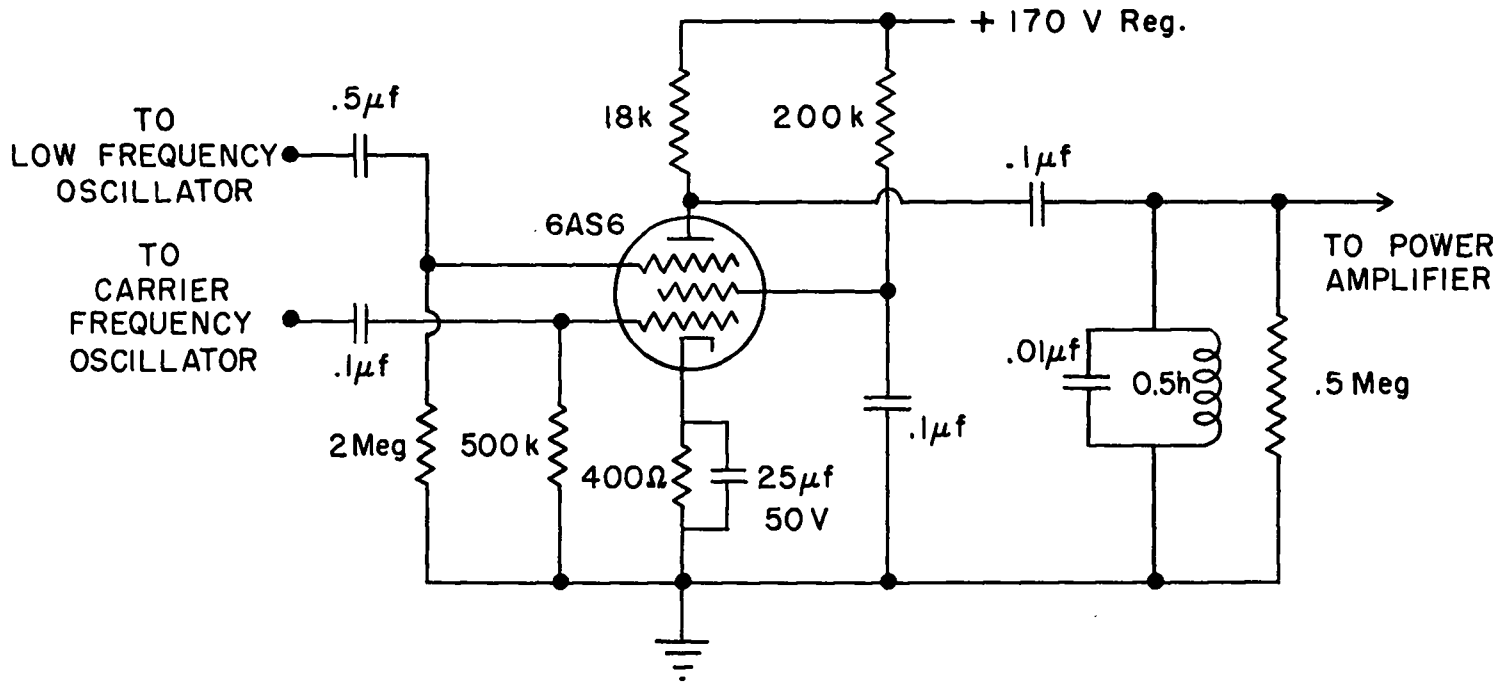

Fig. A2. Schematic diagram of mixer circuit.